Contribution of understory evaporation in a tropical wet forest during the dry season

César Dionisio Jiménez–Rodríguez[1,2], Miriam Coenders–Gerrits[1], Jochen Wenninger[1,3], Adriana Gonzalez–Angarita[4], and Hubert Savenije[1]

[1]Delft University of Technology. Water Resources Section. Stevinweg 1, 2628 CN Delft, The Netherlands.
[2]Tecnológico de Costa Rica. Escuela de Ingeniería Forestal. 159-7050, Cartago, Costa Rica.
[3]Department of Water Science and Engineering, IHE Delft Institute for Water Education, The Netherlands
[4]Independent Researcher

Correspondence: César Dionisio Jiménez–Rodríguez (cdjimenezcr@gmail.com)

Abstract. Tropical wet forests are complex ecosystems with a large number of plant species. These environments are characterized by a high water availability throughout the whole year and a complex canopy structure. However, how the different sections of the canopy contribute to total evaporation is poorly understood. The aim of this work is to estimate the total evaporation flux and differentiate the contribution among canopy layers of a tropical wet forest in Costa Rica. Monitoring the fluxes during the dry season by making use of the energy balance to quantify the fluxes and stable water isotopes to trace the sources of water vapor. Total evaporation was 275.5 mm and represents 55.9 % of the recorded precipitation (498.8 mm), with 11.7 % of the precipitation being intercepted and evaporated along the forest canopy. The understory beneath 8 m contributed with 23.6 % of the evaporation and almost half of it comes from the first 2 m of the understory. Stable water isotope signatures show different soil water sources depending on the plant type. Palms make use of a water source with an isotope signature similar to precipitation and throughfall. Soil water with a fractionated signature is used by trees, bushes and lianas. The isotope signature of water vapor samples overlap among different heights, but it was not possible to make use of the keeling plot method due to the similar isotope signature of the possible sources of water vapor as well as the high water concentration even on the dryer days.

1 Introduction

Total evaporation (E) of forest ecosystems includes water vapor originated from transpiration (E_t), soil evaporation (E_s) and the intercepted water evaporated from wet surfaces (E_i) (Roberts, 1999; Savenije, 2004; Shuttleworth, 1993). Evaporation from tropical forests export more than $1000 \, mm \, yr^{-1}$ of water to the atmosphere (Lion et al., 2017; Loescher et al., 2005; Sun et al., 2016). Partitioning of E is usually focused on the differentiation among E_t, E_s and E_i (Kool et al., 2014; Moore et al., 2018; Xiao et al., 2018). However, the contributions of different sections of the canopy in forest ecosystems are often not considered and are not yet fully understood. The differentiation of E fluxes according to the vertical forest structure had been performed in savanna woodlands and boreal forests (Heijmans et al., 2004; Iida et al., 2009; Scott et al., 2003; Yepez et al., 2003). However, in tropical regions, the vegetation is more complex than the aforementioned ecosystems (savanna woodlands and boreal forests)

and little data concerning the differentiation between understory and overstory evaporation is available (Aparecido et al., 2016; Loescher et al., 2005; Read, 1968).

In tropical forest ecosystems (TFE) the available radiation along the canopy determines the photosynthesis rates and consequently the E_t flux (Hogan and Kattan, 2002). The high radiation received by the overstory in tropical forests allow the emergent trees to transpire more water (Aparecido et al., 2016). Differences in forest evaporation between wet and dry seasons depend on energy and water availability, respectively. Water availability during the wet season does not limit the forest evaporation which depends mostly on the available energy along the canopy gradient (Hogan and Kattan, 2002; Loescher et al., 2005). Contrary to the wet season, the dry season experiences a strong reduction in the precipitation rates triggering physiological responses on the trees. One of these responses is the increment of litterfall (Peters, 2016; Raich, 2017), which depends on precipitation and wind conditions. This temporal drop of leaves during dry season allows the creation of a thinner canopy layer respect to the canopy in the wet season, which can alter the transpiration of understory species such as *Geonoma cuneata* H. Wendl. ex Spruce or *Piper arieianum* C.DC. which exploit the most shaded microsites (Chazdon, 1986, 1992). Thus most of the total evaporation is coming from the overstory during the dry season (Kunert et al., 2017). The understory environment of tropical moist forests is highly variable. This layer receives up to 4 % of the radiation received by the overstory, while canopy gaps can receive 4.3 times more radiation (Tymen et al., 2017) and almost three times higher vapor pressure deficit (Fetcher et al., 1985). These conditions can induce larger transpiration rates as consequence of the plant physiological response to rise in air temperature and vapor pressure deficit (Adelman et al., 2008; Hogg and Hurdle, 1997). This determines the small daily contribution of the understory heat fluxes to the net radiation. However, during days with low net radiation this contribution can be significant at ecosystem level (Loescher et al., 2005). Additionally, the soil water reservoir used by understory shrubs and overstory trees differ. Shrub plants are more dependant on soil water, whereas the trees can access deeper water reservoirs (Ghimire et al., 2018). The number of plant species in TFE can exceed $50\,\mathrm{species\,ha^{-1}}$ (Eilu et al., 2004; Naidu and Kumar, 2016) with densities above $500\,\mathrm{trees\,ha^{-1}}$(Crowther et al., 2015). Also, the heterogeneous spatial aggregation of tree species in TFE (Volkov et al., 2005) increases the number of variables that influences the E_t flux. This increases the number of E_t sources, making it difficult to differentiate between other evaporation fluxes such as E_s or E_i.

The introduction of stable water isotopes in hydrology allowed the refinement of evaporation partitioning (Miralles et al., 2011; Wang et al., 2014). Thus complementing the hydrometric data and providing information about the source of water vapor as a descriptor of the evaporation process (Blyth and Harding, 2011; Dubbert et al., 2017; Silvertown et al., 2015). Stable isotope signatures (δ^{18}O and δ^2H) of different soil water reservoirs may differ due to isotope fractionation, as well as mixing and diffusion processes (Kendall and McDonell, 1998; Hsueh et al., 2016; Sprenger et al., 2016). These processes happen throughout the soil profile with differences in magnitude. Soil evaporation drives the isotopic fractionation of soil water at the superficial soil layers (Dawson and Simonin, 2011; Sutanto et al., 2012). The soil evaporation rate is affected by the presence of different vegetation types or ground layer types (Magliano et al., 2017; Sprenger et al., 2017; Raz-Yaseef et al., 2010). This will change the spatial distribution of isotope signatures with augmented differences because of the enriched isotope signature

of throughfall water reaching the forest floor (Allen et al., 2016; Dawson and Simonin, 2011). Plant water uptake has been considered as a non-fractionation process (Ehleringer and Dawson, 1992; Guo et al., 2016) except for plant species growing in saline or xeric environments (Ellsworth and Williams, 2007). However, recent evidence has shown that tree species such as *Pinus sylvestris* L., *Quercus subpyrenaica* Villar, *Persea americana* Mill., *Fagus sylvatica* L. and *Populus euphratica* Oliv. are

5 able to fractionate the isotope signatures of xylem water (Barbeta et al., 2019; Martín-Gómez et al., 2016; Vargas et al., 2017; Zhao et al., 2016). This arises the question if tropical trees do modify the isotope signature of xylem water, as a response to their plasticity to seasonal changes despite their similar root distribution (Schwendenmann et al., 2015). Different vegetation types (e.g, trees, plam trees, lianas) determine partly the plant root system (Groff and Kaplan, 1988) and with it, the capacity to access specific soil water reservoirs. The transpired water has heavier isotope signatures than xylem water as a consequence

10 of the photosynthesis process (Dubbert et al., 2014; Yakir and Sternberg, 2000), differing from the water source used by the plant. This provides a tool to trace or compare the different sources of water vapor in the air.

The structural complexity of TFE is defined by environmental variables such as altitude, climate and geomorphology (Holdridge et al., 1967; Gomez, 1986; Hartshorn, 2002; Guariguata and Ostertag, 2002). The forest canopy can be segmented

15 into four layers according to vegetation height and light requirements. First, the overstory includes all the trees fully illuminated at the top of the canopy. It is followed by the understory which is composed of woody plants located in the shade beneath the overstory. Third, the ground layer includes all seedlings, herbaceous vegetation and small shrubs. Finally, the forest floor includes the uppermost layer of soil (O Horizon) and the litter layer lying on it (Nadkarni et al., 2004; Parker, 1995). Tropical canopies have a wide number of epiphytes growing on the tree tops along the canopy that influence the effective precipitation,

20 water uptake and E processes (Ah-Peng et al., 2017; Cavelier and Vargas, 2002; Gotsch et al., 2016; Porada et al., 2018; Zotz, 2016). Thus allowing the tall canopies to create a microclimate bellow its shadow (Fitzjarrald and Moore, 1995; Frey et al., 2016; Nakamura et al., 2017). These differences are linked to the energy balance variation along the forest profile, resulting in changes of total evaporation (Ehleringer and Dawson, 1992). Most of the evaporation studies in the tropics focus on yearly patterns (Baldocchi and Ryu, 2011; Calder et al., 1986; da Rocha et al., 2009; Loescher et al., 2005; Schellekens et al., 2000),

25 the wet season (Read, 1968; Wright et al., 2017) or time windows of less than one day to study specific processes such as aerodynamic conductance (Holwerda et al., 2012). But few attempts deepening the knowledge of dry season evaporation has been found (Harper et al., 2014). Tropical forests are highly sensitive to water variability (Tan et al., 2013) and understory light availability (Brenes-Arguedas et al., 2011), which are the main factors defining the distribution of plant species. This because tree seedlings are prompted to use water dripping by short, low-intensity rain events and condensation of occasional fog im-

30 mersion during the dry season (Fu et al., 2016; Liu et al., 2010; Obregon et al., 2011). Consequently, changes in the canopy conditions can modify the understory composition and with it the future forest evaporation. The aforementioned underlines the need to provide more information about the evaporation process during the dry season in tropical forests, as well as the role played by understory vegetation during forest evaporation. This work aims (1) to estimate the total evaporation flux during the dry season in a tropical wet forest, (2) to differentiate the contribution among canopy layers depending on their location

35 with the canopy, (3) to define the contribution of plant transpiration to the dry season evaporation at the forest level, and (4) to

describe the temporal dynamics of the stable isotope signatures during the dry season. To study this, we made use of the energy balance to quantify the fluxes and stable water isotopes to trace the sources of water vapor.

2   Methodology

2.1   Study Site

La Selva Biological Station (LSBS) is located on the Caribbean lowlands of Costa Rica (N: $10°26'0'' - $ W: $83°59'0''$) (Figure 1). This region has a mean annual precipitation of $4351\,\mathrm{mm\,yr^{-1}}$, with a monthly precipitation of more than $100\,\mathrm{mm\,month^{-1}}$ (Loescher et al., 2005). A short dry season is present in this region between February and April and it is characterized by a reduction of precipitation without experiencing a water deficit (Sanford Jr. et al., 1994; Lieberman and Lieberman, 1987). Monthly precipitation during the dry and wet season is $193.7\,\mathrm{mm\,month^{-1}}$ and $419.2\,\mathrm{mm\,month^{-1}}$, respectively. The mean annual temperature is $26.3\,°\mathrm{C}$ with a mean daily difference of $9.5\,°\mathrm{C}$ between the lowest and the highest temperature. The potential evaporation (E_p) accounts for $1585\,\mathrm{mm\,yr^{-1}}$ (Figure 2). The research station is covered by a series of old growth and secondary forests, as well as small forest plantations of different species and mixed plots (Figure 1).
(Putman et al., 2019)

The monitoring period included the dry season of 2018 for 62 days between 2018-1-25 and 2018-3-26. During this period the meteorological data was collected continuously and the water sampling was done during 3 different periods: 2018-01-30 to 2018-02-09 (sampling period A), 2018-02-19 to 2018-02-26 (sampling period B) and 2018-03-19 to 2018-03-25 (sampling period C). This study was carried out at the Major Research Infrastructure plot (MRI–plot) which has an area of 1 ha of old growth forest located on the middle terrace of the Puerto Viejo river (Sanford Jr. et al., 1994). The MRI–plot is situated in the upper section of a small hill facing South–West towards an affluent of the Puerto Viejo river. The soil is classified as Inceptisol (Andic Humidotropept) under the USDA classification system (Sollins et al., 1994). This plot has 88 species among trees, lianas and palms with more than $10\,\mathrm{cm}$ of diameter (see Appendix A). Tree density was $371\,\mathrm{trees\,ha^{-1}}$ in 2017 with $60.6\,\%$ of the trees within 10–$20\,\mathrm{cm}$ diameter. The most abundant species are the palm *Welfia regia* H.Wendl. and the tree *Pentaclethra macroloba* (Willd.) Kuntze with $56\,\mathrm{trees\,ha^{-1}}$ and $43\,\mathrm{trees\,ha^{-1}}$, respectively. Based on data from Tang et al. (2012), the average leaf area index (LAI) in 2005 of the plot was $3.56\,\mathrm{m^2\,m^{-2}}$ (Figure 1). Also, this plot is located within an area of small changes of top canopy height and a neutral change of tree biomass fixation (Dubayah et al., 2010). Canopy structure on the MRI–plot was split into 3 layers. The lower understory (lu) ranges from the ground surface up to $2\,\mathrm{m}$ height, it includes the ground surface, the litter layer and small shrubs. The upper understory (uu) goes up to $10\,\mathrm{m}$ height covering the crowns of medium palms, tall bushes and small trees. The overstory (ov) is the tallest canopy layer and it includes the crowns of the tallest trees of the plot (see Appendix A).
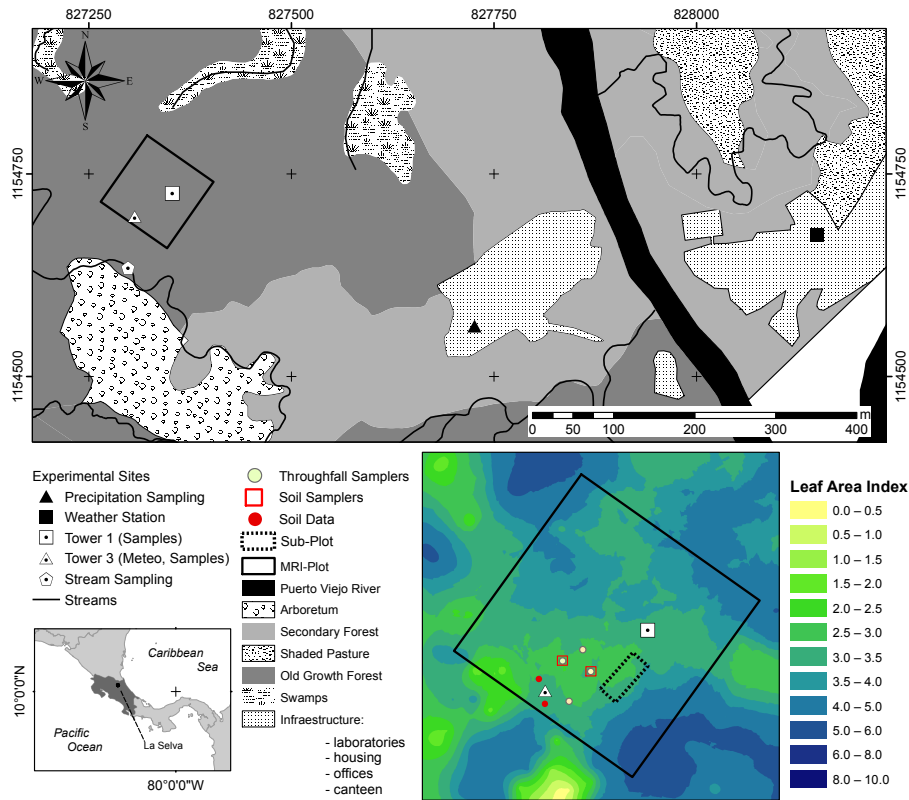
Figure 1. Location of sampling points and the Major Research Infrastructure (MRI–plot) plot at La Selva Biological Station in Puerto Viejo de Sarapiquí, Costa Rica. The land cover map shows the location of the MRI–plot in the Old Growth Forest and the bottom left image depicts the leaf area index (LAI) distribution in the plot.

2.2 Instrumentation

A meteorological station is located 750 m East from the MRI–plot (Figure 1). This station monitors precipitation, air temperature, relative humidity, solar radiation, photosynthetic active radiation, atmospheric pressure, leaf wetness, wind speed and wind direction (Table B1). All sensors are controlled by a Campbell Scientific© data logger, averaging the data over 15 min
5   time intervals and storing it automatically on an online server at the research station. The MRI–plot has 3 research towers with different heights (Tower 1: 34 m, Tower 2: 25 m (under repair during the experiment) and Tower 3: 43 m). Tower 3 is located within a canopy depression of around 400 m^2, and the other two towers allow the access to the forest canopy at the center of the plot (Figure 1). A series of sensors were placed along Tower 3 to monitor different meteorological variables during the study period. Air temperature and relative humidity were installed 1.5 m away from the tower structure at 2 m, 10 m, 37 m
10   and 43 m height; and protected with a radiation shield (ONSET®; RS3-B). Precipitation, solar radiation and photosynthetic active radiation were measured at the highest point of Tower 3 (Table B1). Soil temperature, soil moisture and solar radiation
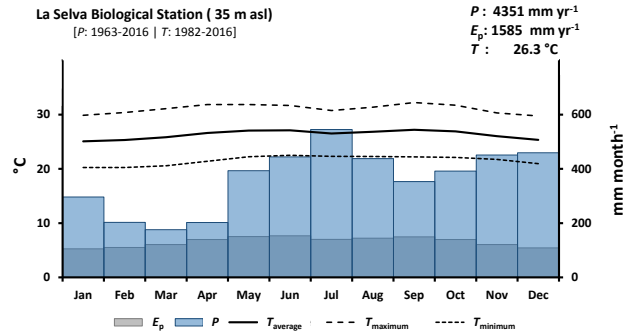
Figure 2. Climate diagram of La Selva Biological Station based on records of 54 years of precipitation (P) and 35 years of temperature (T) (Source: https://tropicalstudies.org/). The potential evaporation (E_p) was estimated with the temperature data and Thornthwaite equation (Thornthwaite, 1948).

were measured at ground level near the base of the tower. The radiation data was recorded with a Campbell Scientific$^©$ data logger (model: CR10x) every 15 min, soil temperature was recorded with a HOBO 4-channel data logger (ONSET$^®$ part code: U12-008) and the other sensors with a HOBO USB Micro Station (ONSET$^®$ part code: H21-USB) every 5 min.

5   Throughfall measurements were carried out at ground level with 15 rain gauges, 12 of them distributed within a sub plot of 200 m^2 (Figure 1) to estimate the bulk throughfall and 3 additional ones placed around Tower 3 to collect daily samples. The measurements were carried out every 24 hr before 7:00 a.m. When isolated rain events happened during the day, the precipitation was measured right after the event. Throughfall was measured in mL with a measuring cylinder of 500 mL with a scale of 0.5 mL. All volumes were translated into mm of water according to the rain gauge surface area. Leaf area index (Γ, m^2 m^{-2}) 10   was determined with hemispherical pictures collected at the raingauge locations within the MRI plot at 50 cm height from the ground. These images were processed with the Gap Light Analyzer (GLA) software (Frazer et al., 1999). All dasometric data of the MRI–plot was provided by the scientific team of LSBS. This data set includes the scientific names of all trees, palms and lianas with more than 10 cm diameter measured at 1.3 m height, as well as the branching heights (m) and tree diameters (cm).

15   2.3   Water Sampling

Different sets of liquid samples were collected at the MRI–plot, in a stream located 50 m downhill the MRI–plot, and at an open area located 400 m South–East from the MRI–plot (Figure 1). Samples of bulk precipitation were collected at the open area on an event basis to determine the isotope variation from individual rainfall events, while overnight precipitation was collected the next day before 6:00 a.m. The samples were collected manually and the reservoir was replaced immediately after 20   the measurement. The additional set of 4 rain gauges collecting bulk throughfall were placed around Tower 3 and sampled on a daily basis or shorter if it was possible. Soil water from the unsaturated zone was collected on a daily basis with soil mois-

6

ture samplers (Eijkelkamp part number: 19.21.SA) of 10 cm length, with a porous polymer of $0.15 \mu m$ diameter. Soil water sampling was carried out at 2 locations around Tower 3, extracting the samples from 5 cm and 15 cm depth in each location. The first 0.5 mL of every sampling were discarded to reduce the contamination from previous soil water extractions. Stream samples were sampled daily during the low flows at the end of the sampling period as a proxy of the groundwater signature.

5   This as a consequence of the absence of boreholes near the MRI-plot. Water vapor samples were collected with a test tube of 30 mL of borosilicate immersed in an isolated container of 500 mL filled with dry ice (-70 °C). The collection was performed at least every three hours depending on the meteorological conditions and dry ice availability during the sampling period. The samples were collected at Tower 3 at 43 m height. Transpired water was collected from the canopy of different plant species surrounding the towers. These samples were collected with polyethylene bags at least every 6 hr and transferred immediately to

10   1.5 mL borosilicate vials. Xylem water was extracted daily from branches or exposed roots at midday for four types of plants: palms (17 samples from 5 species), trees (21 samples from 11 species), bushes (17 samples from 10 species), and lianas (12 samples from 5 species). Detailed information on the sampled species can be found in the supplemental material. The sampled plants were selected randomly according to the plant type from all the individuals within the MRI-plot. The bark of each sample was removed before the water extraction. The xylem sample was placed within a 50 mL test tube with an insert of 30 mL

15   and a DURAPORE® membrane filter (PES-45/25, 0.45 μm, HV). The water was extracted through centrifugation at 5000 rpm for 30 min, transferring immediately the extracted water to 1.5 mL vials. All liquid samples were stored at 6°C, whilst xylem water was stored at -10 °C to prevent the decomposition of the dissolve organics in the sample and the formation of fungi until the water samples were analyzed.

2.4   Energy Fluxes

20

The latent heat flux ($\rho \lambda E$, W m^{-2}) was determined using the energy balance equation (Equation 1) from the ground up to 2 m, 8 m and 43 m (Figure 3). This equation is based on the vertical transport of heat, neglecting the advected energy due to the lack of more detailed measurements (e.g, eddy covariance system). However, considering the tower location away from treefall gaps and at a hill top minimizes major effects of understory canopy advection (Loescher et al., 2005). The net radiation (R_n, W m^{-2})

25   was calculated with equation 2 applying an albedo (a) value of 0.12 according to Loescher et al. (2005) for this forest type and incoming short wave radiation ($R_{\downarrow \mathrm{S}}$). Incoming ($R_{\downarrow \mathrm{L}}$) and outgoing ($R_{\uparrow \mathrm{L}}$) long wave radiation (W m^{-2}) were determined for every time step (see Appendix C). Ground heat flux (G, W m^{-2}) was calculated with equation 3 using the temperature difference (dT) between the soil temperature at 5 cm depth and the superficial soil temperature (T_s0) (see Appendix D). A soil thermal conductivity (k) of 1.58 W m^{-1} °C^{-1} (Pielke, 2013) was used to determine G considering the soil clay content and

30   soil moisture condition of more than 0.40 m^3 m^{-3} during the study period. The sensible heat flux (H, W m^{-2}) was determined using equation 4, where T_a is the air temperature (°C) at the different heights, ρ_a is the air density (kg m^{-3}), c_p is the specific heat of the air (1.013 × 10^{-3} MJ kg^{-1} °C^{-1}), and r_a (s m^{-1}) is the aerodynamic resistance to heat transfer (see Appendix E).

$$\rho\lambda E = R_\mathrm{n} - H - G \tag{1}$$

$$R_\mathrm{n} = (1-a)R_{\downarrow\mathrm{S}} - R_{\uparrow\mathrm{L}} + R_{\downarrow\mathrm{L}} \tag{2}$$

5

$$G = k\frac{\mathrm{d}T}{\mathrm{d}z} \tag{3}$$

$$H = -\rho_\mathrm{a}c_\mathrm{p}\frac{T_\mathrm{a} - T_{\mathrm{s}0}}{r_\mathrm{a}} \tag{4}$$
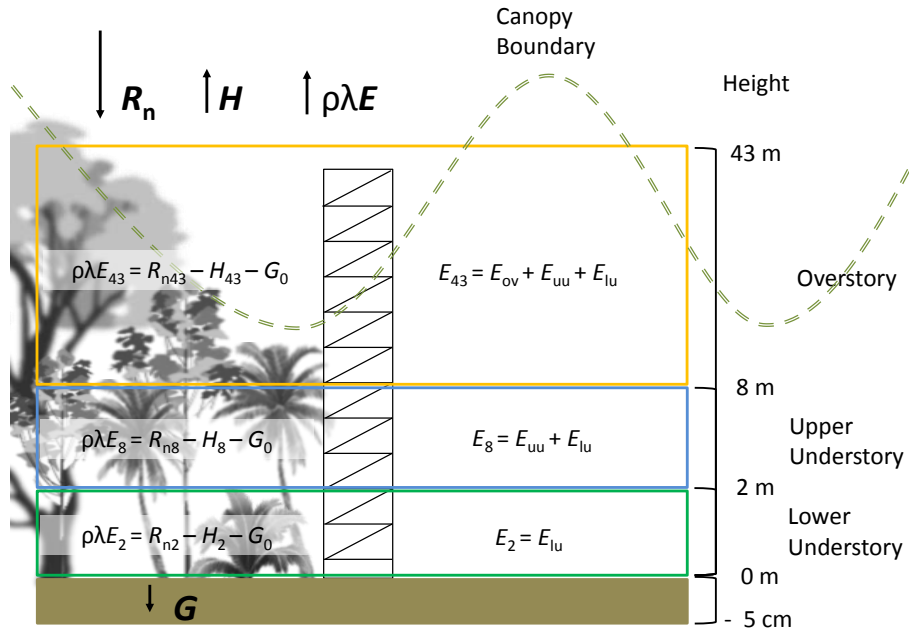
Figure 3. Diagram showing the distribution of canopy layers applied for the partitioning of energy and evaporation fluxes. This diagram also shows the components used for the estimation of the energy balance and its relationship with the estimates of evaporation.

10 **2.5 Isotopic Analysis**

Relative isotope concentration of deuterium (δ^2H) and oxygen–18 (δ^{18}O) with respect to the Vienna Standard Mean Ocean Water (VSMOW) were measured with a Liquid Water Isotope Analyzer (LWIA; model 912-0008) from Los Gatos Research

8

(LGR). We used the software LIMS 10.083 for lasers (Coplen, 2000) during the calibration, correction and determination of stable isotope signatures of the analyzed samples. The relative concentrations were determined following Equation 5 (Craig, 1961), where δ represents the relative concentration (‰) of the stable isotopes δ^2H or $\delta^{18}O$, R is defined as the stable isotope ratio ($^2H/^1H$ or $^{18}O/^{16}O$) of the standard water (R_{standard}) and the sample (R_{sample}). Equation 6 determines the line-conditioned excess (lc-excess) based on the Local Meteoric Water Line (LMWL) defined for La Selva Biological Station by Sánchez-Murillo et al. (2013) as $\delta^2H = 14.03 + 8.48\,\delta^{18}O$.

$$\delta = \left(\frac{R_{\text{sample}}}{R_{\text{standard}}} - 1\right) \tag{5}$$

$$\text{lc} - \text{excess} = \delta^2H - 8.48 * \delta^{18}O - 14.03 \tag{6}$$

The "Keeling method" (Equation 7) was used to determine the contribution of transpiration to the atmospheric water vapor signature of total evaporation (Keeling, 1958; Xiao et al., 2018; Yakir and Sternberg, 2000; Zhang et al., 2010). This method applies the mass balance equation assuming that atmospheric water vapor concentration of the ecosystem (C_{eco}) has the stable isotope signature of δ_{eco} as a result of the mixture of a background atmospheric concentration (C_a) with stable isotope signature of δ_a and water vapor contributed by ecosystem transpiration with an isotope siganture of δ_t. The intercept of this equation represents the net contribution of the ecosystem transpiration.

$$\delta_{\text{eco}} = C_a(\delta_a - \delta_t)(1/C_{\text{eco}}) + \delta_t \tag{7}$$

2.6 Data Analysis

Data processing and analysis were performed with the software R (R Core Team, 2017). All data collected from the sensors were summarized in 15 minutes time intervals to be comparable with the data from the meteorological station of LSBS. The evaporation contribution of the overstory (ov), upper understory (uu) and lower understory (lu) layers was estimated with equations 8–10. Also, the vapor pressure deficit (VPD) was calculated in kPa based on the difference between saturation vapor pressure (e_s)na and actual vapor pressure (e_a) calculated based on the air temperature (T_a) and dew temperature (T_{dew}) of each height. The lc-excess of the samples was used to determine the presence of statistical differences among sample types and the temporal differences within each sample type. As the samples did not follow a normal distribution, a non-parametric analysis was applied. The presence of differences in lc-excess among and within sample types was determined with a Kruskal–Wallis test and the pairwise comparisons were carried out with a Wilcoxon rank sum test.

$$E_2 = E_{\text{lu}} \tag{8}$$

$$E_8 = E_{\mathrm{uu}} + E_{\mathrm{lu}} \tag{9}$$

$$E_{43} = E_{\mathrm{ov}} + E_{\mathrm{uu}} + E_{\mathrm{lu}} \tag{10}$$

3 Results

3.1 Meteorological and Canopy Conditions

Canopy openness and LAI at the MRI-plot were $14.4 \pm 3.4\,\%$ and $2.6 \pm 0.3\,\mathrm{m^2 m^{-2}}$, respectively. During the dry season some trees species experienced a partial loss of leaves (e.g, *P. macroloba*, *Pterocarpus* sp. or *Virola koschnyi* Warb.), this reduces locally the LAI at the end of the sampling period. Rain events during the monitoring period of 62 days had a random distribution, recording a total precipitation of $536.2\,\mathrm{mm}$ (see Appendix G). After 2018-02-01, the rain events intensity experienced a diminution, while the frequency and length of dry periods increased after this date. The occurrence of precipitation affects the VPD, registering maximum values above $2.0\,\mathrm{kPa}$ during the hottest and driest days (Figure G1). The wind was predominantly from the South–East, with an average magnitude of $0.97\,\mathrm{m\,s^{-1}}$ and a maximum of $4.34\,\mathrm{m\,s^{-1}}$. The low average is a consequence of the high frequency of wind speed lower than $2\,\mathrm{m\,s^{-1}}$ and the wide presence of calms. These calms ($u < 0.25\,\mathrm{m\,s^{-1}}$) are present during $27.8\,\%$ of the monitoring period. Daily air temperature oscillates between $17.8\,^{\circ}\mathrm{C}$ and $32.5\,^{\circ}\mathrm{C}$. The presence of rains reduces the vapor pressure deficit (VPD) which does not exceed $3\,\mathrm{kPa}$.

Air temperature differs among canopy heights and between day and night times (Figure 4). At $43\,\mathrm{m}$ and $8\,\mathrm{m}$ height the air temperature has a daily range of more than $10\,^{\circ}\mathrm{C}$, while at $2\,\mathrm{m}$ height the range is smaller ($< 10\,^{\circ}\mathrm{C}$). However, night time conditions along the canopy profile keep the same pattern without strong differences. Superficial soil temperature does not have differences between day and night time, showing the same range of temperatures. However, the differences during day and night time are driven by the median temperature as a consequence of energy dynamics at ground level.

The VPD at the forest canopy changes with respect to the height. VPD at $43\,\mathrm{m}$ height registered the largest values along the monitoring period during day time, droping below $1.0\,\mathrm{kPa}$ at night (Figure 4). VPD day time conditions at $8\,\mathrm{m}$ height are similar to those at $43\,\mathrm{m}$. Beneath the canopy at $2\,\mathrm{m}$ height the VPD have a similar trend to night conditions at $43\,\mathrm{m}$ height with values not larger than $1.0\,\mathrm{kPa}$. Thus reflects the saturated air conditions close to the forest floor despite the high air temperatures at the site, as it is evidenced by the larger frequency of VPD with $0\,\mathrm{kPa}$. Soil moisture conditions at the MRI-plot oscillates between $0.42\,\mathrm{m^3\,m^{-3}}$ and $0.48\,\mathrm{m^3\,m^{-3}}$, without differences between day and night time conditions.

Daily variation of relative humidity along the canopy profile differs depending on the canopy height. During sunny days, the conditions at $43\,\mathrm{m}$ shows are the driest reaching a lower point of $45.2\,\%$ and only goes to $100\,\%$ during rainfall events. The

average relative humidity at 43 m height is 80.9 ±14.3 %. At 8 m height, the relative humidity has an average of 90.1 ±11.3 % with the driest point of 52.3 %. Close to the forest floor, the relative humidity remains close to saturation even during sunny days. At 2 m height, the average relative humidity is 97.2 ± 4.8 % with the driest point of 71.0 % during the driest day.

3.2 Fluxes

5 Between 2018-01-26 and 2018-03-25 a total amount of 492.8 mm of precipitation was recorded, with 4 days of more than 20 mm d^{-1} (Figure 5). Daily measurements of throughfall performed manually at the MRI-plot show that the canopy is able to intercept 11.7 % of the accumulated precipitation (see Appendix H). This interception includes the effect of the 3 canopy layers, which remain wet 61.2 % of the time according to the leaf wetness sensor. Most of the events registered an interception fraction between 0.38 to 0.40. It is important to mention the lack of stem flow measurements at the MRI-plot due to the

10 diversity of plant types and species, as well as the high tree density. This can result in an overestimation of the interception in no more than 2.0 % of precipitation for tropical forests (Cavelier and Vargas, 2002; Tobón Marin et al., 2000; Sá et al., 2016). Soil moisture conditions during the study period remain stable with few minor changes during the monitoring period (Figure 4). The larger values observed in soil moisture are the result of the large amount of throughfall during rain events.

15 $R_{\downarrow S}$ varies depending on the location along the canopy. At 43 m height the R_n has a homogeneous frequency during day time, reaching a maximum value close to 1130 W m^{-2}. While at 8 m and 2 m the frequency of larger $R_{\downarrow S}$ (> 500 W m^{-2}) is sporadic reaching not more than 400 W m^{-2} and 100 W m^{-2}, respectively. The sporadic presence of $R_{\downarrow S}$ is due to the presence of sunbeams filtering through the canopy openings. The reduction of $R_{\downarrow S}$ is linked to the attenuation of the $R_{\downarrow S}$ before reaching the forest floor due to the canopy layers. Forest canopy absorbs, reflects and diffuses more than 95 % of $R_{\downarrow S}$. This attenuation

20 influences the energy availability on the understory and forest floor (Figure 4). The effective energy reaching the forest floor drives the G daily variations, allowing the soil to store up to 32.3 W m^{-2} (Figure 4). This energy is released at night with fluxes up to 39.6 W m^{-2}. This pattern makes G the most important energy flux during night periods at the MRI-plot. Net radiation along the forest canopy profile decreases its magnitude from top to bottom. R_{n43m} had a maximum of 1000.8 W m^{-2}, while the R_{n2m} is just a fraction of this flux. Net radiation at 43 m, 8 m and 2 m during clear nights had similar fluxes, however this

25 pattern differs when rainy conditions are present (see Appendix G). Those conditions allows R_{n2} to transfer less energy to the atmosphere than R_{n8} and R_{n43}.

At 2 m height H does not have strong changes oscillating between -50 W m^{-2} and 100 W m^{-2} during day time, while night time have 0 W m^{-2} most of the time (Figure 4). This flux increases its magnitude on the upper forest layers on day and night

30 time. Most important differences between 8 m and 43 m are based on the maximum H that can be reached. At 8 m and 43 m do not reach 300 W m^{-2}. The frequency peak of H observed along the three heights during day time are linked at the sporadic showers experienced during the monitoring period (see Appendix G). The residuals from the energy balance equations applied to the three canopy layers (Equation 1) represents the $\rho\lambda E$. This flux has strong differences among the canopy heights (Figure 4) where at 43 m the $\rho\lambda E$ goes from -100 W m^{-2} to 910 W m^{-2}, while at 8 m and 2 m height the minimum $\rho\lambda E$ is almost the

same (-67.5 W m^{-2} and -66.5 W m^{-2}, respectively).
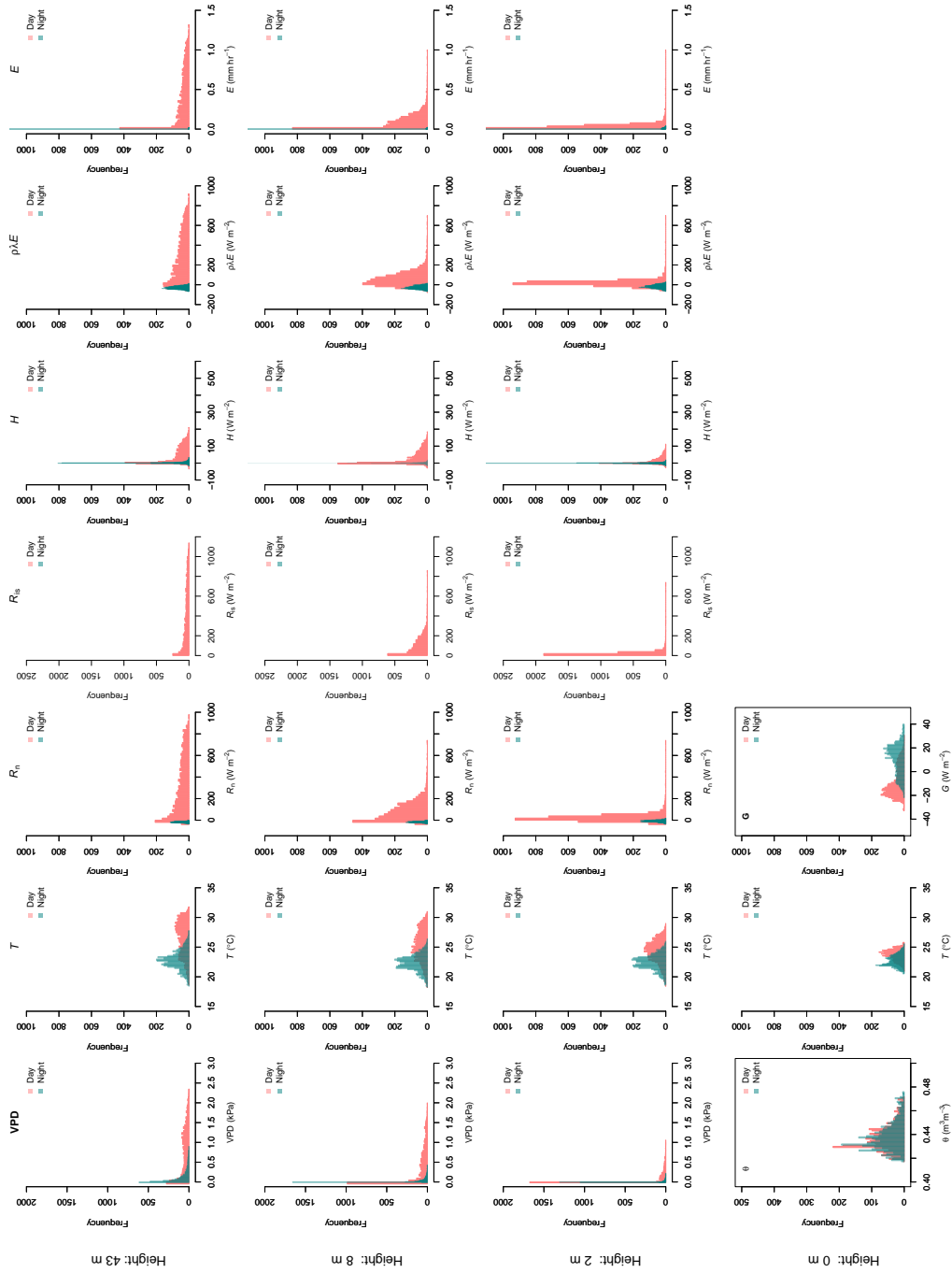
Figure 4. Histograms of the data collected during 62 days of monitoring along the canopy profile of the forest. The variables vapor pressure deficit (VPD), soil moisture (θ), air and soil temperature (T), as well as the energy fluxes (R_n, G, R_{is}, H, $\lambda\rho E$) and evaporation (E) at 43 m, 8 m, 2 m and 0 m height are compared during day and night time. Day time is defined as the period between 06:00 and 18:00 hours and night time between 18:00 and 06:00 hours. Negative values of $\lambda\rho E$ were considered as 0 mm hr^{-1} of E.

13
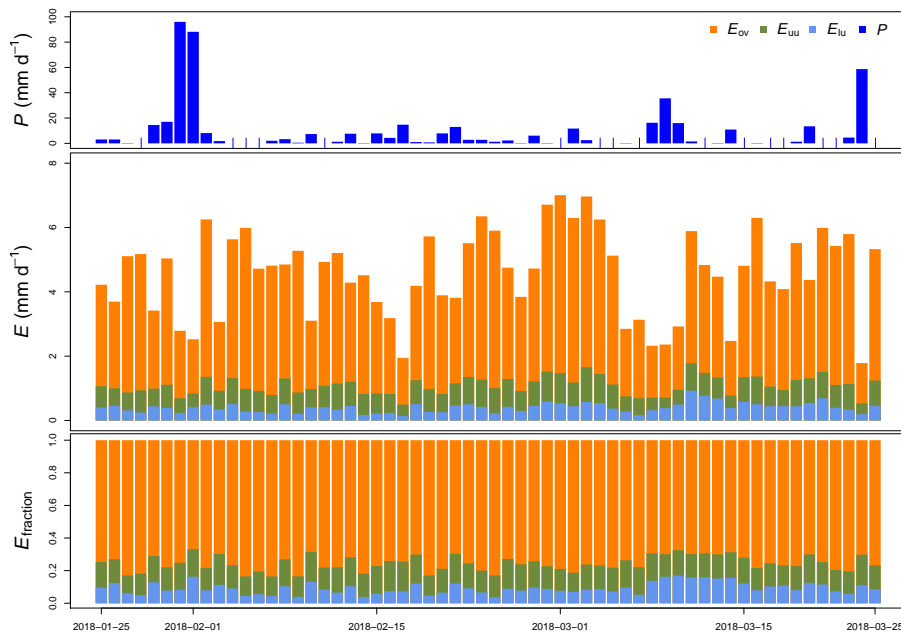
Figure 5. Measured precipitation (P), estimated evaporation (E) and its fraction (E_{fraction}) per canopy layer at La Selva Biological Station (LSBS) during the monitoring period from 2018-01-25 to 2018-03-25.

Along this period, we estimated an evaporation of 275.5 mm accounting for 55.9 % of the precipitation registered at the MRI-plot. A portion of 24.3 mm is originated from 2 m height and 40.7 mm from between 2 m and 8 m height (Figure 5). The contribution of individual canopy layers to evaporation varies among days. The presence of large precipitation events reduces the evaporation (e.g, from 2018-01-31 to 2018-02-01), meanwhile periods with continuous wet conditions but small rain events allows the evaporation to increase (e.g, from 2018-02-17 to 2018-03-03). The overstory layer contributes with an average of 66 $\pm$ 8 %, while the upper understory and the lower understory layers contribute with 15 $\pm$ 2 % and 9 $\pm$ 4 %, respectively.

3.3 Isotope Signatures

Figure 6 and 7 show the variability of all the water samples collected at the MRI-plot. Precipitation samples are located on the LMWL defined for La Selva Biological Station by Sánchez-Murillo et al. (2013), with a slight fractionated signature with respect to the LMWL (Figure 6). These differences in isotope signature is linked to the presence of more convective rain events during the dry season. Isotope signatures of precipitation and throughfall samples overlap, however the precipitation samples have a wider variability than throughfall samples for both isotopes. Throughfall samples have a more homogeneous isotope signature with fewer outliers than precipitation. Soil water signature at 5 cm and 10 cm depth has exactly the same pattern as the LMWL, with only 1 sample with a fractionated signature at 10 cm depth. The lack of fractionation in soil water and the high values of soil moisture depict a low proportion of soil evaporation during the sampling period. The samples of stream

water collected in the stream nearby the plot have an isotope signature that matches with the LMWL. However, the isotope signature differs widely from the precipitation, throughfall and soil water samples collected on the same period.

Transpired water samples have a more fractionated signature with respect to the xylem water (Figure 7). Despite the presence of fractionated xylem water, it does not match with the soil water signature (χ^2: 324.04, p-value < 0.001). Samples of transpired water have a wide variation on their isotopic signatures (Figure 6). Transpired water samples of trees, bushes and palms show a similar pattern among them. This pattern has a lumped group of samples with an isotope signature slightly fractionated with respect to the LMWL and some fractionated samples linked to the dryer days. The samples of transpired water collected in the lianas have a different pattern than the other plant types with a clear fractionation linked with the dryer days.

Xylem water samples show clear differences among plant types. The xylem water from palms has an isotope signature close to the LMWL, depicting a quick access to rain water that can be stored in the palm trunks. The lianas have access to different water sources differing in their isotope signatures (Figure 6). These sources include water from precipitation, stream water and soil water affected by evaporation not present in the collected samples at the MRI–plot (see Appendix **??**). The isotope signature of the xylem water in trees and bushes depict the use of rain water as well as fractionated water. The bushes show a more fractionated signature than trees. This signature can indicate the access to more superficial soil water ($< 5\,cm$) that can be affected by fractionation.

Temporal differences in lc-excess values were not significant (p $=0.05$) for most of the sample types excepting the soil water at 5 cm depth ($\chi^2 = 25.297$, p $= 0.000$), throughfall ($\chi^2 = 9.614$, p $= 0.008$) and tree transpiration ($\chi^2 = 9.884$, p $= 0.007$). Figure 8 shows the tendency lc-excess for each sampling period per sample type. The main differences in throughfall samples are depicted between the beginning (A) and the end of the monitoring period (C). Samples from the sampling period C showed a more fractionated signature meanwhile the sampling period B has an intermediate value between periods. Soil water at 5 cm shows a clear decreasing trend in lc-excess with the pass of time, increasing considerably the fractionation of soil water signature. Finally, trees transpiration differed between the mid sampling period (B) and the end of the sampling period (C).

Isotope signature of water vapor samples from the 3 sampling heights overlap with each other. These samples have a wide range for both isotopes (δ^2H and $\delta^{18}O$), but only some outliers matches with the xylem water samples. However, few vapor samples overlap with other sample types and only 4 samples at 43 m height and 5 samples from 22 m height overlap with the LMWL. Appendix I shows the keeling plots applied to lc-excess and $\delta^{18}O$ of the air samples collected at 43 m and 22 m height. In both cases, the regression lines are not significant ($p_{value} > 0.05$ and $R^2 \approx 0$). The closeness of water samples exemplifying the source of water vapor (e.g, soil water, transpired water, xylem water) and high absolute humidity during the sampling period affected the goodness of fit.
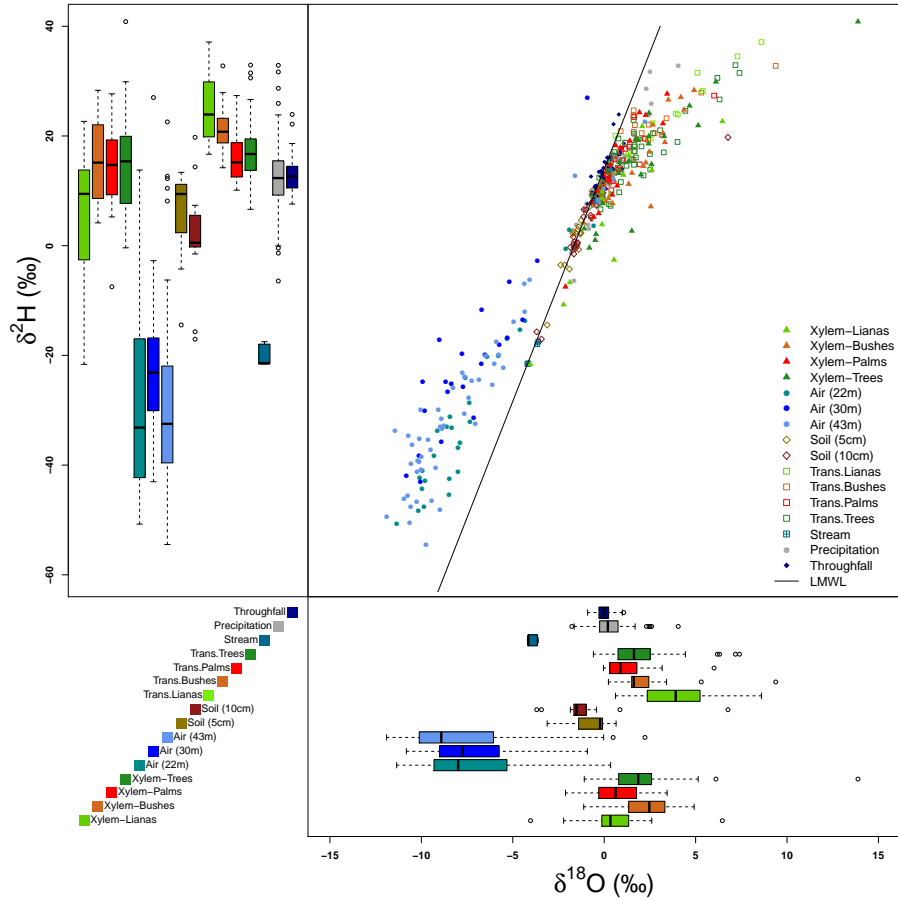
Figure 6. Isotopic signatures of δ^2H and δ^{18}O of all the samples collected at the MRI-plot. Dual isotope plot shows the relationship among the local meteoric water line (LMWL) and all the samples. The box plots of $\delta^2 H$ (upper–left) and δ^{18} (bottom–right) show the distribution of isotope signatures per sample type.

4 Discussion

Evaporation in wet forests is governed by the transpiration process, following a direct link between leaf area index and transpiration (Zhang et al., 2017). However, the role played by the forest canopy during evaporation is more complex and involves processes such as canopy interception (Carlyle-Moses and Gash, 2011; Gerrits et al., 2010) or splash droplet evaporation (Bassette and Bussière, 2008; Murakami, 2006). Broadleaf evergreen forests are able to intercept 13.0 % of the precipitation for subsequent evaporation (Miralles et al., 2010), this matches the observed interception on the MRI-plot with 11.7 % of interception. This proportion accounts for one third of the measured evaporation, leaving the remaining 44.2 % of the evaporated precipitation to canopy transpiration. The distribution of interception along the forest canopy will depend on the accumulated leaf biomass along the canopy, although is not possible to differentiate the proportion of the individual canopy layers. On the
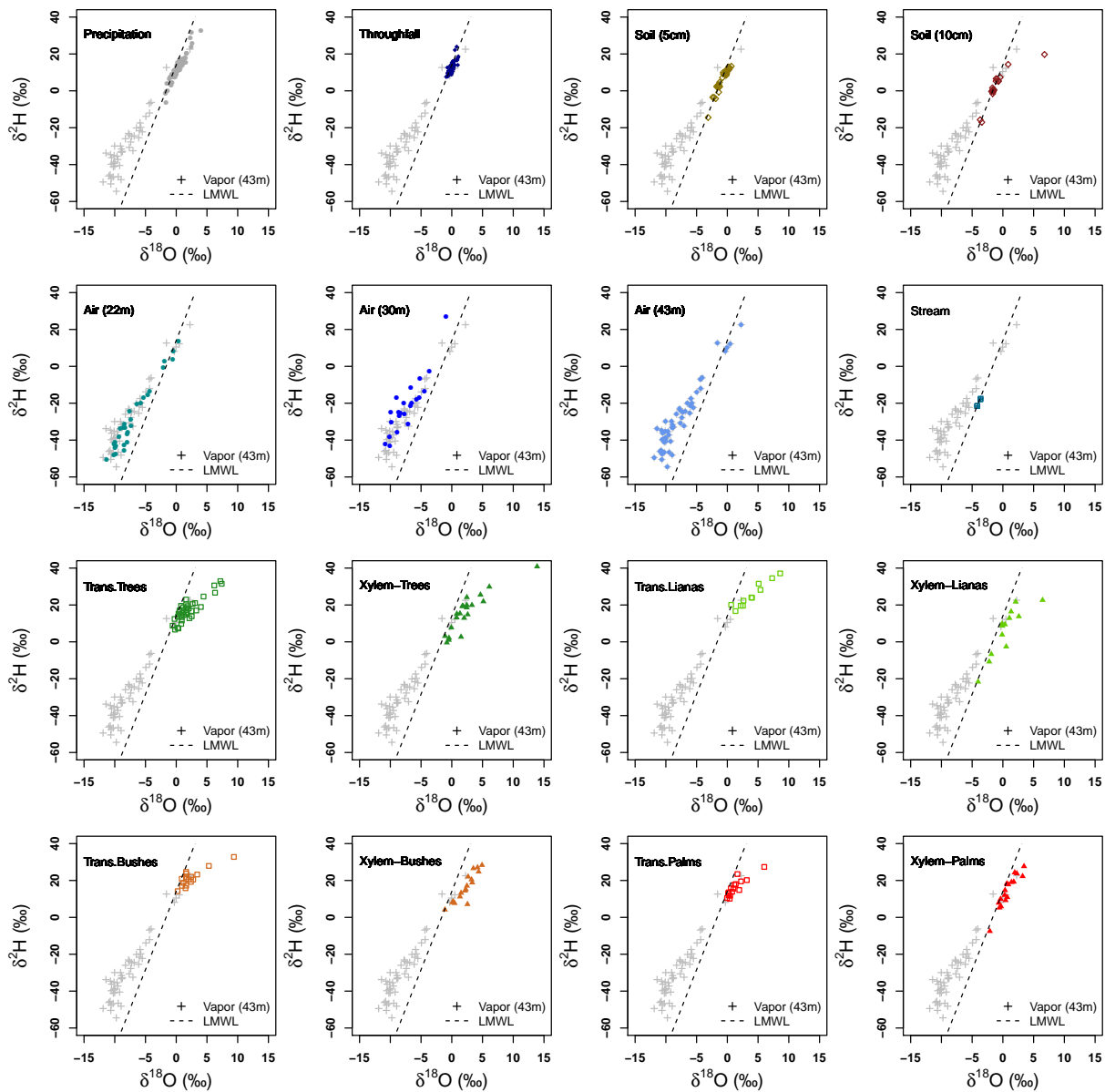
Figure 7. Dual isotope plots of δ^2H and δ^{18}O per sample type collected at La Selva Biological Station. Vapor samples collected at 43 m height and local meteoric water line (LMWL) are used in each plot as references.
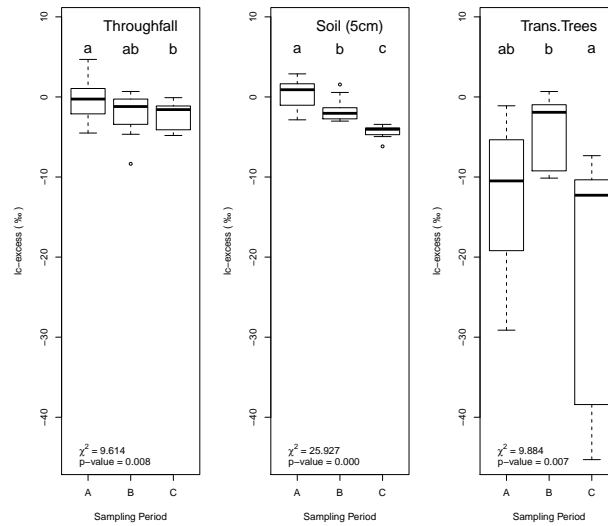
Figure 8. Box plots showing the temporal differences in lc-excess for throughfall, soil water at 5 cm depth, and tree transpiration. The other sample types did not show significant differences (p = 0.05). Sampling periods with the same lower case character per sample type do not differ (p = 0.05).

MRI-plot, 29.4 % of LAI is allocated between 0 and 10 m height, hence the area intercepting precipitation on the understory increases as well as the potential sources of transpiration. Loescher et al. (2005) suggested that transpiration on the lower canopy can affect the lack of ecosystem response to the vapor pressure deficit variations in the upper part in La Selva Biological Station. Thus supports the contribution of 9 % and 15 % of the evaporation by the lower and upper understory recorded during this dry season. Soil evaporation is negligible in respect to transpiration and canopy interception. However, the presence of litter on the forest floor may contribute to the evaporation at 2 m height as part of the forest floor interception. The presence of larger $\rho\lambda E$ at 2 m and 8 m heights are linked to the sunbeams and to their low frequency of occurrence. Negative $\rho\lambda E$ values are linked to the water condensation along the forest canopy. This condensation will trigger the release of latent heat similarly as it happen during the cloud formation processes (Goosse, 2015).

Allen et al. (2016) described the capacity to modify the isotope signature of precipitation when the water passes through the forest canopy. This pattern has been identified in different locations (Allen et al., 2015; Hsueh et al., 2016; Liu et al., 2008). Instead, the throughfall signature at the MRI-plot is more homogeneous than the isotope signature of precipitation. This as a consequence of two factors first, the small number of throughfall samplers used (n = 4), and second the fixed location of each of them. These two factors reduces the possibility to depict the spatial variability of the sampled forest despite the differences on sampling dates. However, the temporal differences among sampling periods show a clear effect of the evaporation process at end of the dry season. The intercepted water is affected by evaporation during the rain events, modifying the isotope signature of the water that drips from the canopy. This water has a more fractionated signature than the precipitation. The higher

temperatures experienced during day time and larger VPD conditions at 43 m and 8 m height drive this change the fractionation of stable water isotopes. Soil water signatures have a larger variability than throughfall signatures, showing lighter signatures than precipitation and throughfall. Soil water does not show the expected fractionation of soil under evaporation processes, where the isotope signature is characterized by heavier fractionated soil water signatures respect to throughfall or precipitation

5   (Allison et al., 1984; Sprenger et al., 2017). This reflects the small contribution to evaporation from the mineral soil, which is supported by the high soil moisture recorded during the monitoring period. However, this does not include the effect of evaporation from litter interception on the forest floor.This effect modifies the soil water isotope signature at 5 cm depth with the development of the dry season. The decreasing trend of lc-excess values shows the effect of the evaporation process that is able to modify the water signature that reaches this depth. This process is cumulative since the evaporation process started

10   modifying the isotope signature at the canopy level, before reaching the litter layer before reaching the mineral soil. This evaporation is linked to the available energy at the lower understory that drives the evaporation process.

Water use by riparian forests in La Selva Biological Station has been linked to groundwater withdrawal (Cadol et al., 2012). Isotope signature of stream water during low flows reflects the isotope signature of groundwater (Blumstock et al., 2015),

15   allowing its use as a proxy to describe the groundwater isotope signature. The collected stream water has a lighter isotope signature than precipitation, throughfall and soil water however, its lc-excess depicts its meteoric origin supporting its use as a reference to describe the groundwater. The stream water signature is lighter than the fractionated water used by trees and bushes, meanwhile, some lianas have a similar signature to stream water. This can lead to link a deepwater use by the lianas, which has been reported in some karstic and seasonal environments (Chen et al., 2015) however, it differs from the findings of

20   (De Deurwaerder et al., 2018) in a similar tropical forest. However, as xylem water and transpired water of lianas have fractionated signatures with respect to the LMWL, but do not match completely with soil neither throughfall samples.Temporal differences showed by transpired water by trees are linked to a variation on the strategies to access different water sources. During the second period of sampling, the rain events were smaller but more frequent than during the first and last sampling periods. This allowed the trees to make use more recently precipitated than the other two periods. Palm and bushes samples

25   are the ones that cover the isotopic range of precipitation and throughfall samples, depicting the use of rain water. Canopy architecture of palm trees allows the concentration of water as stemflow (Germer et al., 2010; Germer, 2013) allowing the quick soil saturation near the root zone with precipitation water. Additionally, palm species have the capacity to store large amounts of water in their stem for their later use (Renninger and Phillips, 2016). This enables these species to have a stable isotope signature close to precipitation water.

30

Tropical bushes and treelets have most of their root system in the upper 20 cm of the soil (Becker and Castillo, 1990), allowing their access to superficial soil water and nutrients. However, it is important to underline that root allocation strategy depends on the species (Jackson et al., 1995). The water signature of xylem water and transpired water of trees and lianas showed a large variability. Differently to palms, tree species are able to develop extensive root systems depending on the nutri-

35   ent availability more than water access in wet environments (Kerfoot, 1963). Whilst the growth strategies of lianas allow them

to have an extensive shallow root system due to their sprout capacity all over the forest floor (Campanello et al., 2016). This root system allow the lianas to have access to superficial soil water (De Deurwaerder et al., 2018), making use of the dripping water after convective fog during the dry season (Liu et al., 2010) and the dry season rains.

5   The overlapping isotope signatures of transpiration and xylem samples with the precipitation water, do not allow to identify proportion of individual sources of water vapor. The highly variable water vapor concentrations during the gas sampling and signature closeness of possible water vapor sources did not allow neither to identify individual sources such as transpiration or evaporation. Determining the source of water vapor with techniques such as the keeling method did not work for this monitoring as a consequence of two factors. First, the similar isotope signatures of the possible sources of water vapor. Secondly, the
10   high concentration of water molecules even in the dryer days. The keeling method has been applied in conditions with clear differences between the sources of water vapor such as in semiarid environments (Yepez et al., 2003, 2005), homogeneous plantations (Sun et al., 2014) or comparing between inland and lake evaporation (Yamanaka and Shimizu, 2007). The presence of few plant species in those cases allowed a more homogeneous signature of transpiration, which is not the case at the MRI-plot which has 88 plant species. Secondly, the similar signature of sources of water vapor (transpired water, soil water of rain
15   water) do not allow a clear differentiation. Finally, the high variability of the water vapor concentration during the different sampling methods did not allow to produce a significant linear regression.

      The structural complexity of a tropical wet forest requires the inclusion of different parameters to better understand the water fluxes such as evaporation. Tackling the structure in terms of canopy layers is possible to homogenized important differences
20   like plant types or number of species. This as a consequence of the larger variability of water sources to which the plants have access or to specific characteristics of the plants that defines how much water can be transpired (Chen et al., 2015; Silvertown, 2004; Silvertown et al., 2015). Traditional evaporation partitioning defines the fluxes in terms of soil evaporation, plant transpiration and evaporation of intercepted water (Roberts, 1999; Savenije, 2004; Shuttleworth, 1993). However, in complex environments partitioning the evaporation in terms of canopy structure can trigger new insights of the hydrological processes
25   involved within them.

      Additionally, it is necessary to understand how individual plant species in tropical environments use different water sources. Water uptake by tropical trees is linked to leaf phenology and transpiration rates (Schwendenmann et al., 2015) however, the use of stable isotopes in xylem water could by affected due to evaporative fractionation during the transport within the plant
30   tissues (Barbeta et al., 2019; Martín-Gómez et al., 2016; Zhao et al., 2016) or selective acquisition (Vargas et al., 2017). This evidence depicts the need to better understand the effect on stable water isotope signatures during the water transport within the plant. Despite the xylem is considered as a close transport system within the plants, the presence of lenticels along the tree stem, twigs and branches allows the gas exchange by the plant growing tissues (Crang et al., 2018; Hopkins and Hüner, 2008). These organs are present in most of the sampled tree species of this study (e.g, *P. macroloba*, *Sacoglottis trichogyna*
35   Cuatrec., *V. koshnyi*, *Virola sebifera* Aubl.). This can trigger additional fractionation processes along with the water transport

in the xylem that can affect the isotope signatures of xylem water, making difficult to point out the water sources for those plants. Also, providing different water vapor signatures to the tree surroundings. This sampling is representative of the riparian forests located within the life zone Tropical Wet Forest according to Holdridge et al. (1967). This because the location in a middle terrace of the Puerto Viejo river allows the formation of riparian forest structures with high dominance of palm species

5 such as *W. regia* and trees like *P. macroloba*. Also, the ample distribution of these two species in Mesoamerica (Borchsenius et al., 1998; Orwa et al., 2009) allows the application of this outcome to other latitudes within the tropics.

5 Conclusions

Forest evaporation during the monitoring period accounted for 55.9 % of the recorded precipitation. The evaporation did no experience an increment or diminution during the dry season, showing no water limitations for the evaporation process at the

10 stand level. The evaporation includes 11.7 % originated from the intercepted water by plant surfaces, which modifies the isotope signature of the water before reaching the ground. The lower evaporation rates recorded (up to $2\,\mathrm{mm\,d^{-1}}$) were linked to rainy conditions and despite this variability, the contribution of the upper and lower understory layers remains constant along the monitoring period (23.6 %). The main differences between lower and upper understory layers rely on the average contribution. The lower understory provides on average a 9.0 % and the upper understory 15.0 % of the evaporation. Ample water availability

15 did not affect the contribution of individual layers. The low variability of soil moisture during this dry season depicts a small contribution to evaporation from forest soil, a pattern that is supported by the lack of fractionated signature of stable water isotopes. The use of keeling plots to differentiate between transpiration and other sources of water vapor was affected by the highly similar signature of sources of water vapor, by the larger number of plant species and the high water concentration and variability. Evaporation processes during the dry season in Tropical wet forests are not restricted by water availability.

20 However, understory plants and palm species can be affected during drought periods due to the reduction of superficial water availability triggered by a diminution of rains and/or changes in water dripping after fog events.

References

Adelman, J. D., Ewers, B. E., and MacKay, D. S.: Use of temporal patterns in vapor pressure deficit to explain spatial autocorrelation dynamics in tree transpiration, Tree Physiology, 28, 647–658, https://doi.org/10.1093/treephys/28.4.647, 2008.

Ah-Peng, C., Cardoso, A. W., Flores, O., West, A., Wilding, N., Strasberg, D., and Hedderson, T. A.: The role of epiphytic bryophytes in interception, storage, and the regulated release of atmospheric moisture in a tropical montane cloud forest, Journal of Hydrology, 548, 665–673, https://doi.org/10.1016/j.jhydrol.2017.03.043, http://www.sciencedirect.com/science/article/pii/S0022169417301853, 2017.

Allen, S. T., Keim, R. F., and McDonnell, J. J.: Spatial patterns of throughfall isotopic composition at the event and seasonal timescales, Journal of Hydrology, 522, 58–66, https://doi.org/10.1016/j.jhydrol.2014.12.029, 2015.

Allen, S. T., Keim, R. F., Barnard, H. R., McDonnell, J. J., and Renée, B. J.: The role of stable isotopes in understanding rainfall interception processes: a review, Wiley Interdisciplinary Reviews: Water, 4, e1187, https://doi.org/10.1002/wat2.1187, 2016.

Allison, G., Barnes, C., Hughes, M., and Leaney, F.: Effect of climate and vegetation on oxygen-18 and deuterium profiles in soils, Isotopes Hydrology, IAEA, Vienna, pp. 105–122, 1984.

An, N., Hemmati, S., and Cui, Y.-J.: Assessment of the methods for determining net radiation at different time–scales of meteorological variables, Journal of Rock Mechanics and Geotechnical Engineering, 9, 239–246, https://doi.org/10.1016/j.jrmge.2016.10.004, 2017.

Aparecido, L. M. T., Miller, G. R., Cahill, A. T., and Moore, G. W.: Comparison of tree transpiration under wet and dry canopy conditions in a Costa Rican premontane tropical forest, Hydrological Processes, 30, 5000–5011, https://doi.org/10.1002/hyp.10960, 2016.

Baldocchi, D. D. and Ryu, Y.: A Synthesis of Forest Evaporation Fluxes – from Days to Years – as Measured with Eddy Covariance, pp. 101–116, Springer Netherlands, Dordrecht, https://doi.org/10.1007/978-94-007-1363-5_5, 2011.

Barbeta, A., Jones, S. P., Clavé, L., Wingate, L., Gimeno, T. E., Fréjaville, B., Wohl, S., and Ogée, J.: Unexplained hydrogen isotope offsets complicate the identification and quantification of tree water sources in a riparian forest, Hydrology and Earth System Sciences, 23, 2129–2146, https://doi.org/10.5194/hess-23-2129-2019, 2019.

Bassette, C. and Bussière, F.: Partitioning of splash and storage during raindrop impacts on banana leaves, Agricultural and Forest Meteorology, 148, 991 – 1004, https://doi.org/10.1016/j.agrformet.2008.01.016, 2008.

Becker, P. and Castillo, A.: Root Architecture of Shrubs and Saplings in the Understory of a Tropical Moist Forest in Lowland Panama, Biotropica, 22, 242–249, https://doi.org/10.2307/2388534, http://www.jstor.org/stable/2388534, 1990.

Blumstock, M., Tetzlaff, D., Malcolm, I., Nuetzmann, G., and Soulsby, C.: Baseflow dynamics: Multi-tracer surveys to assess variable groundwater contributions to montane streams under low flows, Journal of Hydrology, 527, 1021–1033, https://doi.org/10.1016/j.jhydrol.2015.05.019, 2015.

Blyth, E. and Harding, R. J.: Methods to separate observed global evapotranspiration into the interception, transpiration and soil surface evaporation components, Hydrological Processes, 25, 4063–4068, https://doi.org/10.1002/hyp.8409, 2011.

Borchsenius, F., Borgtoft-Pedersen, H., and Baslev, H.: Manual to the Palms of Ecuador. AAU Reports 37. Department of Systematic Botany, University of Aarhus, Denmark in collaboration with Pontificia Universidad Catolica del Ecuador World Checklist of Arecaceae, 1998.

Brenes-Arguedas, T., Roddy, A. B., Coley, P. D., and Kursar, T. A.: Do differences in understory light contribute to species distributions along a tropical rainfall gradient?, Oecologia, 166, 443–456, https://doi.org/10.1007/s00442-010-1832-9, 2011.

Cadol, D., Kampf, S., and Wohl, E.: Effects of evapotranspiration on baseflow in a tropical headwater catchment, Journal of Hydrology, 462-463, 4–14, https://doi.org/10.1016/j.jhydrol.2012.04.060, tropical Hydrology, 2012.

Calder, I., Wright, I., and Murdiyarso, D.: A study of evaporation from tropical rain forest — West Java, Journal of Hydrology, 89, 13 – 31, https://doi.org/10.1016/0022-1694(86)90139-3, 1986.

Campanello, P. I., Manzané, E., Villagra, M., Zhang, Y.-J., Panizza, A. M., di Francescantonio, D., Rodriguez, S. A., Chen, Y.-J., Santiago, L. S., and Goldstein, G.: Carbon Allocation and Water Relations of Lianas Versus Trees, pp. 103–124, Springer International Publishing, Cham, https://doi.org/10.1007/978-3-319-27422-5_5, 2016.

Carlyle-Moses, D. E. and Gash, J. H. C.: Rainfall Interception Loss by Forest Canopies, pp. 407–423, Springer Netherlands, Dordrecht, https://doi.org/10.1007/978-94-007-1363-5_20, 2011.

Cavelier, J. and Vargas, G.: Procesos Hidrológicos, in: Ecología y conservación de bosques neotropicales, edited by Guariguata, M. and Kattan, G., pp. 144–166, Libro Regional Universitario (LUR), 2002.

Chazdon, R. L.: The Costs of Leaf Support in Understory Palms: Economy Versus Safety, The American Naturalist, 127, 9–30, https://doi.org/10.1086/284464, 1986.

Chazdon, R. L.: Photosynthetic plasticity of two rain forest shrubs across natural gap transects, Oecologia, 92, 586–595, https://doi.org/10.1007/BF00317853, 1992.

Chen, Y.-J., Cao, K.-F., Schnitzer, S. A., Fan, Z.-X., Zhang, J.-L., and Bongers, F.: Water-use advantage for lianas over trees in tropical seasonal forests, New Phytologist, 205, 128–136, https://doi.org/10.1111/nph.13036, 2015.

Coplen, T.: A guide for the laboratory information management system (LIMS) for light stable isotopes–Versions 7 and 8: U.S. Geological Survey Open-File Report 00-345, 121 p., https://water.usgs.gov/software/code/geochemical/lims/doc/ofr00345.pdf, 2000.

Craig, H.: Standard for Reporting Concentrations of Deuterium and Oxygen-18 in Natural Waters, Science, 133, 1833–1834, https://doi.org/10.1126/science.133.3467.1833, 1961.

Crang, R., Lyons-Sobaski, S., and Wise, R.: Plant Anatomy: A Concept-Based Approach to the Structure of Seed Plants, Springer, 2018.

Crowther, T. W., Glick, H. B., Covey, K. R., Bettigole, C., Maynard, D. S., Thomas, S. M., Smith, J. R., Hintler, G., Duguid, M. C., Amatulli, G., et al.: Mapping tree density at a global scale, Nature, 525, 201, 2015.

da Rocha, H. R., Manzi, A. O., Cabral, O. M., Miller, S. D., Goulden, M. L., Saleska, S. R., R.-Coupe, N., Wofsy, S. C., Borma, L. S., Artaxo, P., Vourlitis, G., Nogueira, J. S., Cardoso, F. L., Nobre, A. D., Kruijt, B., Freitas, H. C., von Randow, C., Aguiar, R. G., and Maia, J. F.: Patterns of water and heat flux across a biome gradient from tropical forest to savanna in Brazil, Journal of Geophysical Research: Biogeosciences, 114, https://doi.org/10.1029/2007JG000640, 2009.

Dawson, T. E. and Simonin, K. A.: The Roles of Stable Isotopes in Forest Hydrology and Biogeochemistry, pp. 137–161, Springer Netherlands, Dordrecht, 2011.

De Deurwaerder, H., Hervé-Fernández, P., Stahl, C., Burban, B., Petronelli, P., Hoffman, B., Bonal, D., Boeckx, P., and Verbeeck, H.: Liana and tree below-ground water competition—evidence for water resource partitioning during the dry season, Tree Physiology, 38, 1071–1083, https://doi.org/10.1093/treephys/tpy002, 2018.

Dubayah, R. O., Sheldon, S. L., Clark, D. B., Hofton, M. A., Blair, J. B., Hurtt, G. C., and Chazdon, R. L.: Estimation of tropical forest height and biomass dynamics using lidar remote sensing at La Selva, Costa Rica, Journal of Geophysical Research: Biogeosciences, 115, https://doi.org/10.1029/2009JG000933, 2010.

Dubbert, M., Cuntz, M., Piayda, A., and Werner, C.: Oxygen isotope signatures of transpired water vapor: the role of isotopic non-steady-state transpiration under natural conditions, New Phytologist, 203, 1242–1252, https://doi.org/10.1111/nph.12878, 2014.

Dubbert, M., Kübert, A., and Werner, C.: Impact of leaf traits on temporal dynamics of transpired oxygen isotope signatures and its impact on atmospheric vapor, Frontiers in plant science, 8, https://doi.org/10.3389/fpls.2017.00005, 2017.

Eamus, D., Huete, A., and Yu, Q.: Modelling Leaf and Canopy Transpiration and the Soil–Plant–Atmosphere Continuum, in: Vegetation dynamics, edited by Eamus, D., Huete, A., and Yu, Q., chap. 12, pp. 296–320, Cambridge University Press, 2016.

Ehleringer, J. and Dawson, T.: Water uptake by plants: perspectives from stable isotope composition, Plant, Cell & Environment, pp. 1073–1082, https://doi.org/10.1111/j.1365-3040.1992.tb01657.x, 1992.

5 Eilu, G., Hafashimana, D. L. N., and Kasenene, J. M.: Density and species diversity of trees in four tropical forests of the Albertine rift, western Uganda, Diversity and Distributions, 10, 303–312, https://doi.org/10.1111/j.1366-9516.2004.00089.x, 2004.

Ellsworth, P. Z. and Williams, D. G.: Hydrogen isotope fractionation during water uptake by woody xerophytes, Plant and Soil, 291, 93–107, https://doi.org/10.1007/s11104-006-9177-1, 2007.

Fetcher, N., Oberbauer, S. F., and Strain, B. R.: Vegetation effects on microclimate in lowland tropical forest in Costa Rica, International 10 Journal of Biometeorology, 29, 145–155, https://doi.org/10.1007/BF02189035, 1985.

Fitzjarrald, D. and Moore, K.: Physical Mechanisms of heat and mass exchange between forests and the atmosphere, in: Forest Canopies, edited by Lowman, M. and Nadkarni, N., pp. 45–72, academic Press, 1995.

Frazer, G. W., Canham, C., and Lertzman, K.: Gap Light Analyzer (GLA), Version 2.0: Imaging software to extract canopy structure and gap light transmission indices from true-colour fisheye photographs, users manual and program documentation, Simon Fraser University, 15 Burnaby, British Columbia, and the Institute of Ecosystem Studies, Millbrook, New York, 36, 1999.

Frey, S. J. K., Hadley, A. S., Johnson, S. L., Schulze, M., Jones, J. A., and Betts, M. G.: Spatial models reveal the microclimatic buffering capacity of old-growth forests, Science Advances, 2, https://doi.org/10.1126/sciadv.1501392, 2016.

Fu, P.-L., Liu, W.-J., Fan, Z.-X., and Cao, K.-F.: Is fog an important water source for woody plants in an Asian tropical karst forest during the dry season?, Ecohydrology, 9, 964–972, https://doi.org/10.1002/eco.1694, 2016.

20 Germer, S.: Development of near-surface perched water tables during natural and artificial stemflow generation by babassu palms, Journal of Hydrology, 507, 262–272, https://doi.org/10.1016/j.jhydrol.2013.10.026, 2013.

Germer, S., Werther, L., and Elsenbeer, H.: Have we underestimated stemflow? Lessons from an open tropical rainforest, Journal of Hydrology, 395, 169–179, https://doi.org/10.1016/j.jhydrol.2010.10.022, 2010.

Gerrits, A. M. J., Pfister, L., and Savenije, H. H. G.: Spatial and temporal variability of canopy and forest floor interception in a beech forest, 25 Hydrological Processes, 24, 3011–3025, https://doi.org/10.1002/hyp.7712, 2010.

Ghimire, C. P., Lubczynski, M. W., Bruijnzeel, L. A., Zwartendijk, B. W., van Meerveld, H. J. I., Odongo, V. O., and Ravelona, M.: Transpiration and stomatal conductance in a young secondary tropical montane forest: contrasts between native trees and invasive understorey shrubs, Tree Physiology, 38, 1053–1070, https://doi.org/10.1093/treephys/tpy004, 2018.

Gomez, L.: Vegetacion de Costa Rica: Apuntes para una biogeografia Costarricense: vegetacion y clima de Costa Rica., EUNED, 1986.

30 Goosse, H.: The energy balance, hydrological and carbon cycles, in: Climate System Dynamics and Modelling, chap. 2, Cambridge University Press, 2015.

Gotsch, S. G., Nadkarni, N., and Amici, A.: The functional roles of epiphytes and arboreal soils in tropical montane cloud forests, Journal of Tropical Ecology, 32, 455—-468, https://doi.org/10.1017/S026646741600033X, 2016.

Groff, P. A. and Kaplan, D. R.: The relation of root systems to shoot systems in vascular plants, The Botanical Review, 54, 387–422, 35 https://doi.org/10.1007/BF02858417, 1988.

Guariguata, M. and Ostertag, R.: Sucesión secundaria, in: Ecología y conservación de bosques neotropicales, edited by Guariguata, M. and Kattan, G., pp. 591–624, Libro Regional Universitario (LUR), 2002.

Guo, F., juan MA, J., jian Zheng, L., huan Sun, X., hong Guo, X., and lan Zhang, X.: Estimating distribution of water uptake with depth of winter wheat by hydrogen and oxygen stable isotopes under different irrigation depths, Journal of Integrative Agriculture, 15, 891–906, https://doi.org/10.1016/S2095-3119(15)61258-8, 2016.

Harper, A., Baker, I. T., Denning, A. S., Randall, D. A., Dazlich, D., and Branson, M.: Impact of Evapotranspiration on Dry Season Climate in the Amazon Forest, Journal of Climate, 27, 574–591, https://doi.org/10.1175/JCLI-D-13-00074.1, 2014.

Hartshorn, G.: Biogeografía de los bosques neotropicales, in: Ecología y conservación de bosques neotropicales, edited by Guariguata, M. and Kattan, G., pp. 59–82, Libro Regional Universitario (LUR), 2002.

Heijmans, M. M. P. D., Arp, W. J., and Chapin, F. S.: Controls on moss evaporation in a boreal black spruce forest, Global Biogeochemical Cycles, 18, 1–8, https://doi.org/10.1029/2003GB002128, gB2004, 2004.

Hogan, K. and Kattan, J.: La luz solar: consecuencias biológicas y medición, in: Ecología y conservación de bosques neotropicales, edited by Guariguata, M. and Kattan, G., pp. 119–143, Libro Regional Universitario (LUR), 2002.

Hogg, E. H. and Hurdle, P. A.: Sap flow in trembling aspen: implications for stomatal responses to vapor pressure deficit, Tree Physiology, 17, 501–509, https://doi.org/10.1093/treephys/17.8-9.501, 1997.

Holdridge, L. R. et al.: Life zone ecology., Life zone ecology., 1967.

Holmes, T. R. H., Owe, M., De Jeu, R. A. M., and Kooi, H.: Estimating the soil temperature profile from a single depth observation: A simple empirical heatflow solution, Water Resources Research, 44, 1–11, https://doi.org/10.1029/2007WR005994, 2008.

Holwerda, F., Bruijnzeel, L., Scatena, F., Vugts, H., and Meesters, A.: Wet canopy evaporation from a Puerto Rican lower montane rain forest: The importance of realistically estimated aerodynamic conductance, Journal of Hydrology, 414-415, 1–15, https://doi.org/10.1016/j.jhydrol.2011.07.033, 2012.

Hopkins, W. G. and Hüner, N. P.: Introduction to Plant Physiology, Wiley, 2008.

Hsueh, Y.-H., Allen, S. T., and Keim, R. F.: Fine-scale spatial variability of throughfall amount and isotopic composition under a hardwood forest canopy, Hydrological Processes, 30, 1796–1803, https://doi.org/10.1002/hyp.10772, 2016.

Iida, S., Ohta, T., Matsumoto, K., Nakai, T., Kuwada, T., Kononov, A. V., Maximov, T. C., van der Molen, M. K., Dolman, H., Tanaka, H., and Yabuki, H.: Evapotranspiration from understory vegetation in an eastern Siberian boreal larch forest, Agricultural and Forest Meteorology, 149, 1129–1139, https://doi.org/10.1016/j.agrformet.2009.02.003, 2009.

Jackson, P. C., Cavelier, J., Goldstein, G., Meinzer, F. C., and Holbrook, N. M.: Partitioning of water resources among plants of a lowland tropical forest, Oecologia, 101, 197–203, https://doi.org/10.1007/BF00317284, 1995.

Jimenez-Rodriguez, C., Gonzalez-Angarita, A., and Coenders-Gerrits, A.: Meteorological data and isotope signatures of water samples collected at La Selva., https://doi.org/10.4121/uuid:e70993d2-5852-4f63-9aff-39451fbd3fde, 2019.

Keeling, C. D.: The concentration and isotopic abundances of atmospheric carbon dioxide in rural areas, Geochimica et Cosmochimica Acta, 13, 322–334, https://doi.org/10.1016/0016-7037(58)90033-4, 1958.

Kendall, C. and McDonell, J. J., eds.: Chapter 5 - Isotopic Exchange in Soil Water, pp. 137 – 163, Elsevier, Amsterdam, https://doi.org/10.1016/B978-0-444-81546-0.50012-4, 1998.

Kerfoot, O.: THE ROOT SYSTEMS OF TROPICAL FOREST TREES, The Commonwealth Forestry Review, 42, 19–26, http://www.jstor.org/stable/42602976, 1963.

Kool, D., Agam, N., Lazarovitch, N., Heitman, J., Sauer, T., and Ben-Gal, A.: A review of approaches for evapotranspiration partitioning, Agricultural and Forest Meteorology, 184, 56 – 70, https://doi.org/10.1016/j.agrformet.2013.09.003, 2014.

Kunert, N., Aparecido, L. M. T., Wolff, S., Higuchi, N., dos Santos, J., de Araujo, A. C., and Trumbore, S.: A revised hydrological model for the Central Amazon: The importance of emergent canopy trees in the forest water budget, Agricultural and Forest Meteorology, 239, 47–57, https://doi.org/10.1016/j.agrformet.2017.03.002, 2017.

Lieberman, D. and Lieberman, M.: Forest tree growth and dynamics at La Selva, Costa Rica (1969-1982), Journal of Tropical Ecology, 3, 347–358, https://doi.org/10.1017/S0266467400002327, 1987.

Lion, M., Kosugi, Y., Takanashi, S., Noguchi, S., Itoh, M., Katsuyama, M., Matsuo, N., and Shamsuddin, S.-A.: Evapotranspiration and water source of a tropical rainforest in peninsular Malaysia, Hydrological Processes, 31, 4338–4353, https://doi.org/10.1002/hyp.11360, 2017.

Liu, W., Liu, W., Li, P., Duan, W., and Li, H.: Dry season water uptake by two dominant canopy tree species in a tropical seasonal rainforest of Xishuangbanna, SW China, Agricultural and Forest Meteorology, 150, 380–388, https://doi.org/10.1016/j.agrformet.2009.12.006, 2010.

Liu, W. J., Liu, W. Y., Li, J. T., Wu, Z. W., and Li, H. M.: Isotope variations of throughfall, stemflow and soil water in a tropical rain forest and a rubber plantation in Xishuangbanna, SW China, Hydrology Research, 39, 437–449, https://doi.org/10.2166/nh.2008.110, 2008.

Loescher, H., Gholz, H., Jacobs, J., and Oberbauer, S.: Energy dynamics and modeled evapotranspiration from a wet tropical forest in Costa Rica, Journal of Hydrology, 315, 274–294, https://doi.org/10.1016/j.jhydrol.2005.03.040, 2005.

Magliano, P. N., Giménez, R., Houspanossian, J., Páez, R. A., Nosetto, M. D., Fernández, R. J., and Jobbágy, E. G.: Litter is more effective than forest canopy reducing soil evaporation in Dry Chaco rangelands, Ecohydrology, 10, e1879–n/a, https://doi.org/10.1002/eco.1879, 2017.

Martín-Gómez, P., Serrano, L., and Ferrio, J. P.: Short-term dynamics of evaporative enrichment of xylem water in woody stems: implications for ecohydrology, Tree Physiology, 37, 511–522, https://doi.org/10.1093/treephys/tpw115, 2016.

Miralles, D. G., Gash, J. H., Holmes, T. R. H., de Jeu, R. A. M., and Dolman, A. J.: Global canopy interception from satellite observations, Journal of Geophysical Research: Atmospheres, 115, https://doi.org/10.1029/2009JD013530, 2010.

Miralles, D. G., De Jeu, R. A. M., Gash, J. H., Holmes, T. R. H., and Dolman, A. J.: Magnitude and variability of land evaporation and its components at the global scale, Hydrology and Earth System Sciences, 15, 967–981, https://doi.org/10.5194/hess-15-967-2011, 2011.

Moore, G. W., Orozco, G., Aparecido, L. M., and Miller, G. R.: Upscaling transpiration in diverse forests: Insights from a tropical premontane site, Ecohydrology, 11, e1920, https://doi.org/10.1002/eco.1920, 2018.

Murakami, S.: A proposal for a new forest canopy interception mechanism: Splash droplet evaporation, Journal of Hydrology, 319, 72 – 82, https://doi.org/10.1016/j.jhydrol.2005.07.002, 2006.

Nadkarni, N. M., Parker, G. G., Rinker, H. B., and Jarzen, D. M.: CHAPTER 1 - The Nature of Forest Canopies, in: Forest Canopies (Second Edition), edited by Lowman, M. D. and Rinker, H. B., Physiological Ecology, pp. 3–23, Academic Press, San Diego, second edition edn., https://doi.org/10.1016/B978-012457553-0/50005-8, https://www.sciencedirect.com/science/article/pii/B9780124575530500058, 2004.

Naidu, M. T. and Kumar, O. A.: Tree diversity, stand structure, and community composition of tropical forests in Eastern Ghats of Andhra Pradesh, India, Journal of Asia-Pacific Biodiversity, 9, 328 – 334, https://doi.org/https://doi.org/10.1016/j.japb.2016.03.019, 2016.

Nakamura, A., Kitching, R. L., Cao, M., Creedy, T. J., Fayle, T. M., Freiberg, M., Hewitt, C., Itioka, T., Koh, L. P., Ma, K., Malhi, Y., Mitchell, A., Novotny, V., Ozanne, C. M., Song, L., Wang, H., and Ashton, L. A.: Forests and Their Canopies: Achievements and Horizons in Canopy Science, Trends in Ecology Evolution, 32, 438–451, https://doi.org/10.1016/j.tree.2017.02.020, 2017.

Nakshabandi, G. A. and Kohnke, H.: Thermal conductivity and diffusivity of soils as related to moisture tension and other physical properties, Agricultural Meteorology, 2, 271–279, https://doi.org/10.1016/0002-1571(65)90013-0, 1965.

Obregon, A., Gehrig-Downie, C., Gradstein, S. R., Rollenbeck, R., and Bendix, J.: Canopy level fog occurrence in a tropical lowland forest of French Guiana as a prerequisite for high epiphyte diversity, Agricultural and Forest Meteorology, 151, 290–300, https://doi.org/10.1016/j.agrformet.2010.11.003, 2011.

Orwa, C., Mutua, A., Kindt, R., Jamnadass, R., and Anthony, S.: AgroforestreeDatabase: a tree reference and selection guide version 4.0., http://old.worldagroforestry.org/treedb/index.php, 2009.

Parker, G. G.: Structure and microclimate of forest Canopies, in: Forest Canopies, edited by Lowman, M. and Nadkarni, N., pp. 73–106, Academic Press, San Diego, first edition edn., 1995.

Peters, T.: Climatic Types of Water Balances in the Tropics, Tropical Forestry Handbook, pp. 405–412, 2016.

Pielke, R.: Mesoscale Meteorological Modeling, International Geophysics, Elsevier Science, https://books.google.nl/books?id=ExlFulltapcC, 2013.

Porada, P., Van Stan, J. T., and Kleidon, A.: Significant contribution of non-vascular vegetation to global rainfall interception, Nature Geoscience, 11, 563, https://doi.org/10.13031/2013.19812, 2018.

Putman, A. L., Fiorella, R. P., Bowen, G. J., and Cai, Z.: A Global Perspective on Local Meteoric Water Lines: Meta-analytic Insight Into Fundamental Controls and Practical Constraints, Water Resources Research, 55, 6896–6910, https://doi.org/10.1029/2019WR025181, 2019.

R Core Team: R: A Language and Environment for Statistical Computing, R Foundation for Statistical Computing, Vienna, Austria, https://www.R-project.org/, 2017.

Raich, J. W.: Temporal Variability of Soil Respiration in Experimental Tree Plantations in Lowland Costa Rica, Forests, 8, https://doi.org/10.3390/f8020040, 2017.

Raz-Yaseef, N., Rotenberg, E., and Yakir, D.: Effects of spatial variations in soil evaporation caused by tree shading on water flux partitioning in a semi-arid pine forest, Agricultural and Forest Meteorology, 150, 454 – 462, https://doi.org/10.1016/j.agrformet.2010.01.010, 2010.

Read, R. G.: Evaporative Power in the Tropical Forest of the Panama Canal Zone, Journal of Applied Meteorology, 7, 417–424, https://doi.org/10.1175/1520-0450(1968)007<0417:EPITTF>2.0.CO;2, 1968.

Renninger, H. J. and Phillips, N. G.: Palm Physiology and Distribution in Response to Global Environmental Change, pp. 67–101, Springer International Publishing, Cham, https://doi.org/10.1007/978-3-319-27422-5_4, 2016.

Roberts, J.: Plants and water in forests and woodlands, pp. 181–236, Routledge, 1999.

Sá, J. a. H. M., Chaffe, P. L. B., and Quillet, M. J. J.: The influence of the interception process on the precipitation quality in a catchment covered by subtropical Atlantic Forest, RBRH, 21, 742–751, https://doi.org/10.1590/2318-0331.011616045, 2016.

Sánchez-Murillo, R., Esquivel-Hernández, G., Welsh, K., Brooks, E. S., Boll, J., Alfaro-Solís, R., and Valdés-González, J.: Spatial and Temporal Variation of Stable Isotopes in Precipitation across Costa Rica: An Analysis of Historic GNIP Records, Open Journal of Modern Hydrology, https://doi.org/10.4236/ojmh.2013.34027, 2013.

Sanford Jr., R. L., Paaby, P., Luvall, J. C., and Phillips, E.: Climate, geomorphology, and aquatic systems., in: La Selva. Ecology and natural history of a Neotropical Rainforest, edited by McDade, L. A., Bawa, K. S., Hespenheide, H. A., and Hartshorn, G. S., chap. 3, pp. 19–33, The University of Chicago Press, 1994.

Savenije, H. H. G.: The importance of interception and why we should delete the term evapotranspiration from our vocabulary, Hydrological Processes, 18, 1507–1511, https://doi.org/10.1002/hyp.5563, 2004.

Schellekens, J., Bruijnzeel, L. A., Scatena, F. N., Bink, N. J., and Holwerda, F.: Evaporation from a tropical rain forest, Luquillo Experimental Forest, eastern Puerto Rico, Water Resources Research, 36, 2183–2196, https://doi.org/10.1029/2000WR900074, 2000.

Schwendenmann, L., Pendall, E., Sanchez-Bragado, R., Kunert, N., and Hölscher, D.: Tree water uptake in a tropical plantation varying in tree diversity: interspecific differences, seasonal shifts and complementarity, Ecohydrology, 8, 1–12, https://doi.org/10.1002/eco.1479, 2015.

Scott, R. L., Watts, C., Payan, J. G., Edwards, E., Goodrich, D. C., Williams, D., and Shuttleworth, W. J.: The understory and overstory partitioning of energy and water fluxes in an open canopy, semiarid woodland, Agricultural and Forest Meteorology, 114, 127–139, 2003.

Shuttleworth, W.: Evaporation, in: Handbook of hydrology, edited by Maidment, D. R., chap. 4, pp. 4.1–4.53, Mc-Graw Hill, Inc., New York, 1993.

Silvertown, J.: Plant coexistence and the niche, Trends in Ecology Evolution, 19, 605 – 611, https://doi.org/10.1016/j.tree.2004.09.003, 2004.

Silvertown, J., Araya, Y., and Gowing, D.: Hydrological niches in terrestrial plant communities: a review, Journal of Ecology, 103, 93–108, https://doi.org/10.1111/1365-2745.12332, 2015.

Sollins, P., Sancho M., F., Mata Ch., R., and Sanford Jr., R. L.: Soils and soil process research, in: La Selva. Ecology and natural history of a Neotropical Rainforest, edited by McDade, L. A., Bawa, K. S., Hespenheide, H. A., and Hartshorn, G. S., chap. 4, pp. 34–53, The University of Chicago Press, 1994.

Sprenger, M., Leistert, H., Gimbel, K., and Weiler, M.: Illuminating hydrological processes at the soil-vegetation-atmosphere interface with water stable isotopes, Reviews of Geophysics, 54, 674–704, https://doi.org/10.1002/2015RG000515, 2016.

Sprenger, M., Tetzlaff, D., and Soulsby, C.: Soil water stable isotopes reveal evaporation dynamics at the soil–plant–atmosphere interface of the critical zone, Hydrology and Earth System Sciences, 21, 3839–3858, https://doi.org/10.5194/hess-21-3839-2017, 2017.

Sun, G., Domec, J., and Amatya, D.: Forest evapotranspiration: measurement and modelling at multiple scales., in: Forest hydrology: processes, management and assessment., edited by Amatya, D., Williams, T., Bren, L., and Jong, C., CAB International, https://doi.org/10.1079/9781780646602.0032, 2016.

Sun, S., Meng, P., Zhang, J., Wan, X., Zheng, N., and He, C.: Partitioning oak woodland evapotranspiration in the rocky mountainous area of North China was disturbed by foreign vapor, as estimated based on non-steady-state 18O isotopic composition, Agricultural and Forest Meteorology, 184, 36–47, https://doi.org/10.1016/j.agrformet.2013.08.006, 2014.

Sutanto, S. J., Wenninger, J., Coenders-Gerrits, A. M. J., and Uhlenbrook, S.: Partitioning of evaporation into transpiration, soil evaporation and interception: a comparison between isotope measurements and a HYDRUS-1D model, Hydrology and Earth System Sciences, 16, 2605–2616, https://doi.org/10.5194/hess-16-2605-2012, 2012.

Tan, Z.-H., Cao, M., Yu, G.-R., Tang, J.-W., Deng, X.-B., Song, Q.-H., Tang, Y., Zheng, Z., Liu, W.-J., Feng, Z.-L., Deng, Y., Zhang, J.-L., Liang, N., and Zhang, Y.-P.: High sensitivity of a tropical rainforest to water variability: Evidence from 10 years of inventory and eddy flux data, Journal of Geophysical Research: Atmospheres, 118, 9393–9400, https://doi.org/10.1002/jgrd.50675, 2013.

Tang, H., Dubayah, R., Swatantran, A., Hofton, M., Sheldon, S., Clark, D. B., and Blair, B.: Retrieval of vertical LAI profiles over tropical rain forests using waveform lidar at La Selva, Costa Rica, Remote Sensing of Environment, 124, 242 – 250, https://doi.org/https://doi.org/10.1016/j.rse.2012.05.005, http://www.sciencedirect.com/science/article/pii/S0034425712002088, 2012.

Thornthwaite, C. W.: An approach toward a rational classification of climate, Geographical Review, 38, 55–94, https://doi.org/10.2307/210739, 1948.

Tobón Marin, C., Bouten, W., and Sevink, J.: Gross rainfall and its partitioning into throughfall, stemflow and evaporation of intercepted water in four forest ecosystems in western Amazonia, Journal of Hydrology, 237, 40–57, https://doi.org/10.1016/S0022-1694(00)00301-2, 2000.

Tymen, B., Vincent, G., Courtois, E. A., Heurtebize, J., Dauzat, J., Marechaux, I., and Chave, J.: Quantifying micro-environmental variation in tropical rainforest understory at landscape scale by combining airborne LiDAR scanning and a sensor network, Annals of Forest Science, 74, 32, https://doi.org/10.1007/s13595-017-0628-z, 2017.

Van Wijk, W. and Scholte Ubing, D.: Radiation, in: Physics of plant environment, edited by Van Wijk, W., pp. 62–101, Amsterdam, Netherlands: North-Holland Publishing Company, 1963.

Vargas, A. I., Schaffer, B., Yuhong, L., and Sternberg, L. d. S. L.: Testing plant use of mobile vs immobile soil water sources using stable isotope experiments, New Phytologist, 215, 582–594, https://doi.org/10.1111/nph.14616, 2017.

Volkov, I., Banavar, J. R., He, F., Hubbell, S. P., and Maritan, A.: Density dependence explains tree species abundance and diversity in tropical forests, Nature, 438, 658, 2005.

Wang, L., Good, S. P., and Caylor, K. K.: Global synthesis of vegetation control on evapotranspiration partitioning, Geophysical Research Letters, 41, 6753–6757, https://doi.org/10.1002/2014GL061439, 2014GL061439, 2014.

Wright, J. S., Fu, R., Worden, J. R., Chakraborty, S., Clinton, N. E., Risi, C., Sun, Y., and Yin, L.: Rainforest-initiated wet season onset over the southern Amazon, Proceedings of the National Academy of Sciences, 114, 8481–8486, https://doi.org/10.1073/pnas.1621516114, 2017.

Xiao, W., Wei, Z., and Wen, X.: Evapotranspiration partitioning at the ecosystem scale using the stable isotope method—A review, Agricultural and Forest Meteorology, 263, 346–361, https://doi.org/10.1016/j.agrformet.2018.09.005, 2018.

Yakir, D. and Sternberg, L. d. S. L.: The use of stable isotopes to study ecosystem gas exchange, Oecologia, 123, 297–311, https://doi.org/10.1007/s004420051016, 2000.

Yamanaka, T. and Shimizu, R.: Spatial distribution of deuterium in atmospheric water vapor: Diagnosing sources and the mixing of atmospheric moisture, Geochimica et Cosmochimica Acta, 71, 3162–3169, https://doi.org/10.1016/j.gca.2007.04.014, 2007.

Yepez, E. A., Williams, D. G., Scott, R. L., and Lin, G.: Partitioning overstory and understory evapotranspiration in a semiarid savanna woodland from the isotopic composition of water vapor, Agricultural and Forest Meteorology, 119, 53–68, https://doi.org/10.1016/S0168-1923(03)00116-3, 2003.

Yepez, E. A., Huxman, T. E., Ignace, D. D., English, N. B., Weltzin, J. F., Castellanos, A. E., and Williams, D. G.: Dynamics of transpiration and evaporation following a moisture pulse in semiarid grassland: A chamber-based isotope method for partitioning flux components, Agricultural and Forest Meteorology, 132, 359–376, https://doi.org/10.1016/j.agrformet.2005.09.006, 2005.

Zhang, S., Wen, X., Wang, J., Yu, G., and Sun, X.: The use of stable isotopes to partition evapotranspiration fluxes into evaporation and transpiration, Acta Ecologica Sinica, 30, 201–209, https://doi.org/10.1016/j.chnaes.2010.06.003, 2010.

Zhang, Y., Chiew, F. H. S., Peña Arancibia, J., Sun, F., Li, H., and Leuning, R.: Global variation of transpiration and soil evaporation and the role of their major climate drivers, Journal of Geophysical Research: Atmospheres, 122, 6868–6881, https://doi.org/10.1002/2017JD027025, 2017.

Zhao, L., Wang, L., Cernusak, L. A., Liu, X., Xiao, H., Zhou, M., and Zhang, S.: Significant Difference in Hydrogen Isotope Composition Between Xylem and Tissue Water in Populus Euphratica, Plant, Cell & Environment, 39, 1848–1857, https://doi.org/10.1111/pce.12753, 2016.

Zotz, G.: The Role of Vascular Epiphytes in the Ecosystem, pp. 229–243, Springer International Publishing, Cham, https://doi.org/10.1007/978-3-319-39237-0_9, 2016.

Appendix A: Characterization of the Canopy Layers

Figure A1. Images of the 3 canopy layers defined in this study. A: is the lateral view of the overstory layer ($\sim$10 m–43 m) within the canopy gap. B: is the vertical view of the upper understory layer (between 8 m to 10 m). C: is the lateral view of the lower understory (0–2 m).

Figure A2. Plant densities (plant ha^{-1}) and basal area (m^2 ha^{-1}) of the species with more than 10 cm diameter measured at 1.3 m above the ground. Plant basal area corresponds to the cross section area covered by the stem of each plant. Some bush species are not included in this data set because the individuals do not have the minimum diameter required.

Appendix B: Instrumentation

Table B1. Measurement height of the instrumentation used during the experiment carried out in La Selva Biological Station in both.

Variable	Unit	Instrument	Meteorological Station	Tower 3
Precipitation	$mm\,hr^{-1}$	Raingauge (model: TE525MM)	1.5 m	NA
		Davis® Rain Gauge ONSET® (S-RGD-M002)	NA	45 m
Temperature	°C	HMP45C-L probe	1.5 m	NA
		ONSET® (S-THB-M008)	NA	2 m, 10 m, 37 m, 43 m
Relative Humidity	%	HMP45C-L probe	1.5 m	NA
		ONSET® (S-THB-M008)	NA	2 m, 10 m, 37 m, 43 m
Solar Radiation	$W\,m^{-2}$	LI-COR® pyranometer (LI-200X)	3 m	43 m
		Sylicon Pyranometer (ONSET®, S-LIB-M003)	NA	2 m
Photosynthetic Active Radiation	$\mu mol\,m^{-2}s^{-1}$	LI-COR® quantum sensor (LI-190R)	3 m	43 m
Leaf Wetness	minutes	Campbell Scientific© sensor (237-L)	3 m	NA
Wind Speed Wind Direction	$m\,s^{-1}$ ° of Azimuth	R.M.Young® wind monitor (05103)	10 m	NA
Atmospheric Pressure	hPa	Nova Lynx® barometer (230-P111)	2 m	NA
Soil Moisture	$m^3\,m^{-3}$	ECH$_2$O® EC sensor	NA	-5 cm, -10 cm
Soil Temperature	°C	ONSET® (TMC20-HD)	NA	-5 cm, -10 cm

Note: NA indicates that this device is not available at the meteorological station or the MRI plot.

Appendix C: Long Wave Radiation

The incoming and outgoing long wave radiation were determined with equations C1 and and C2 (An et al., 2017), where σ is the Stefan–Boltzman constant ($5.67 \times 10^{-8}\,W\,m^{-2}\,K^{-4}$) and ϵ_s and ϵ_a are the emissivity factors for soil and air, respectively. For ϵ_s a value of 0.97 (Van Wijk and Scholte Ubing, 1963) was used for wet clay soils. ϵ_a was determined with equation C3 based on air temperature (T_{air}) and air vapor pressure (e_a).

$$L \uparrow = \epsilon_s \sigma (T_s)^4 \tag{C1}$$

$$L \downarrow = \epsilon_a \sigma (T_a)^4 \tag{C2}$$

$$\epsilon_a = 0.7 + 5.95 \times 10^{-4} e_a \exp\left(\frac{1500}{T_{air}+273.15}\right) \tag{C3}$$

5 Appendix D: Superficial Soil Temperature

Superficial soil temperature (T_{s0}, °C) was estimated with equation D1 (Holmes et al., 2008) and the available data of soil temperature at 5 cm depth (T_{s5}). This equation describes the diurnal variations of soil temperature as sine waves depending on the 24 h moving averages of soil temperature (T_a, °C). The daily amplitude (T_A, °C) is defined as the difference between T_{s5} and T_a. The oscillations are determined by the damping depth (ν, m) which is calculated with equation D3. z (m) is the depth difference between the target temperature (T_{s0}) and the source temperature (T_{s5}). The sine pattern depends on the angular frequency (ω, $1\,\mathrm{s}^{-1}$), time (t, s) and ϕ as a constant for phase change. Equation D2 is used to determine ω with τ (s) as the wave period.

$$T_{s0} = T_a + T_A \times e^{\left(\frac{-z}{\nu}\right)} \times sin(\omega t - \frac{z}{\nu} + \phi) \tag{D1}$$

$$\omega = \frac{2\pi}{\tau} \tag{D2}$$

Equation D3 calculates ν with the soil thermal diffusivity (η, $\mathrm{m^2\,s^{-1}}$) and ω. Equation D5 (Nakshabandi and Kohnke, 1965) is used to determine η. Where ρ_s is the soil bulk density of $0.76\,\mathrm{g\,cm^{-3}}$ (Sollins et al., 1994) for the experimental plot. c_s is the specific heat for clay soils ($837.36\,\mathrm{W\,kg^{-1}\,°C^{-1}}$). k is the soil thermal conductivity of $1.58\,\mathrm{W\,m^{-1}\,°C^{-1}}$ (Pielke, 2013).

$$\nu = \sqrt{\frac{2\eta}{\omega}} \tag{D3}$$

$$r = \frac{4\sqrt{23}}{yo} \tag{D4}$$

$$\eta = \frac{k}{\rho_s c_s} \tag{D5}$$

Appendix E: Canopy Aerodynamic Resistance

The aerodynamic resistance (r_a, s m^{-1}) was calculated with equation E1 (Eamus et al., 2016). In this equation, k is the von–Karman constant (0.41), z_r is the reference height (m), d is the zero plane displacement, z_0 is the roughness length and u as the wind speed (m s^{-1}). Equation E2 calculates d with h as the canopy height (m). Leaf area index is represented by Γ (m^2 m^{-2})

$$r_a = \frac{\ln^2\left[\frac{(z_r - d)}{z_0}\right]}{(k^2 u)} \tag{E1}$$

$$d = 0.63 \sigma_\alpha h \tag{E2}$$

$$z_0 = (1 - \sigma_\alpha)z_b + \frac{\sigma_\alpha (h - d)}{3} \tag{E3}$$

$$\sigma_\alpha = 1 - \left(\frac{0.5}{0.5 + \Gamma}\right)\exp\left(-\frac{\Gamma^2}{8}\right) \tag{E4}$$

Appendix F: Wind Speed Estimation

The wind speed (u_{45m}) was estimated based in a previous data set collected at the MRI Plot and the relationship with the meteorological variables collected at the research station during that period. The u_{45m} was estimated with a linear regression model, selecting the parameters with an stepwise forward fitting procedure. Equation F1 determines u_{45m} (m s^{-1}) based on the air temperature at 43 m (T_{43m}) collected in Tower 3, wind speed at 10 m (u_{10m}) and incoming short wave radiation ($R_{\downarrow s}$) measured at the meteorological station. The linear regression has an multiple correlation coefficient (R^2) of 0.786, with a residual error of 0.4084 m s^{-1}. Table F1 shows the coefficients estimated with the linear regression analysis, where all of them have are statistically significant (p < 0.001). Considering the standard error from the estimation, all the estimated u_{45m} values lower than 0.41 m s^{-1} were considered as 0 m s^{-1}.

$$u_{45m} = a + b\,u_{10m} + c\,T_{43m} + d\,R_{\downarrow s} \tag{F1}$$

Table F1. Summary of the linear regression analysis to determine the wind speed above the canopy base on previous measured data from the MRI plot and the meteorological station in La Selva Biological Station. Based in data collected at 30 min intervals in both locations from the year 2012.

Parameter	Coefficient	Standard Error	$t$value	Pr($>$|t|)
a	-3.718×10^{-01}	3.998×10^{-02}	-9.298	$<2 \times 10^{-16}$
b	1.028	5.303×10^{-03}	193.873	$<2 \times 10^{-16}$
c	3.298×10^{-02}	1.745×10^{-03}	18.899	$<2 \times 10^{-16}$
d	-2.155×10^{-04}	1.998×10^{-05}	-10.789	$<2 \times 10^{-16}$

Appendix G: Meteorological conditions at La Selva Biological Station
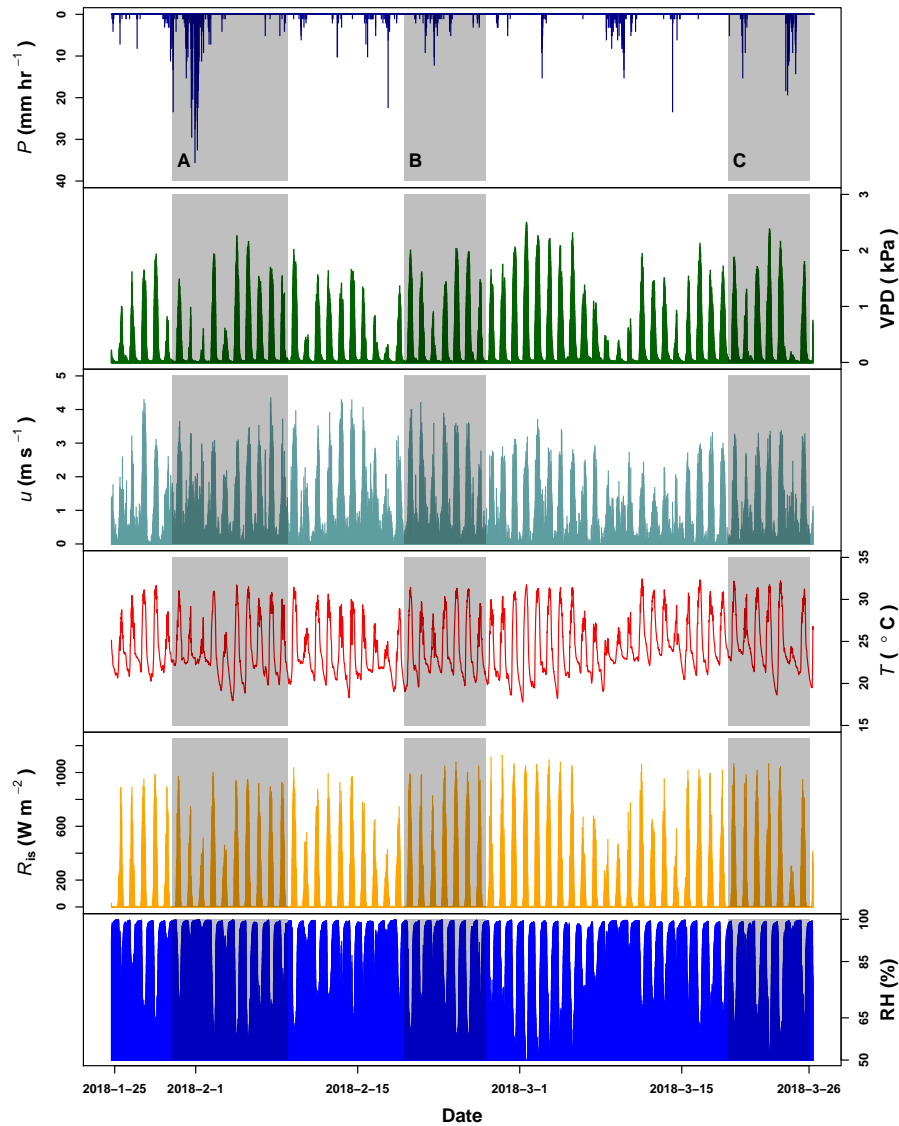
Figure G1. Precipitation (P), vapor pressure deficit (VPD), wind speed (u) and temperature (T) registered by the meteorological station at La Selva Biological Station (LSBS). The monitoring period cover from 2018-01-20 to 2018-03-25. Shadowed areas represent the 3 periods when water samples were collected at the MRI-plot.

Appendix H: Interception of precipitation
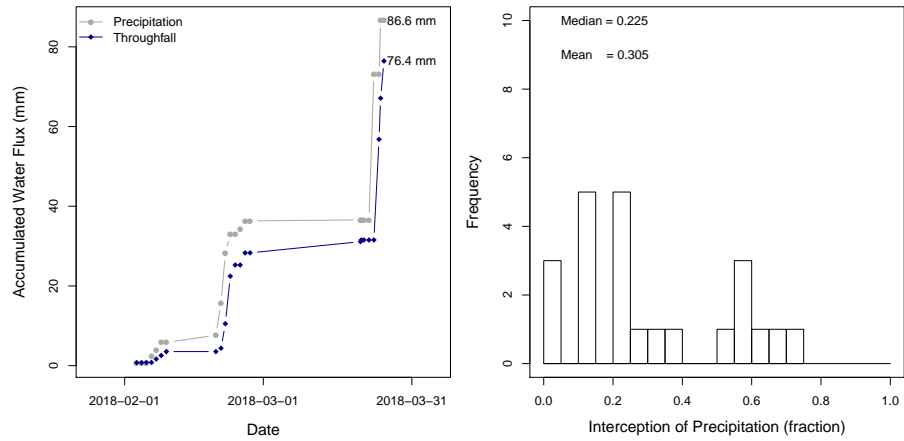
Figure H1. Analysis of the interception of precipitation for the sampling carried out at La Selva Biological Station.

Appendix I: Keeling plots
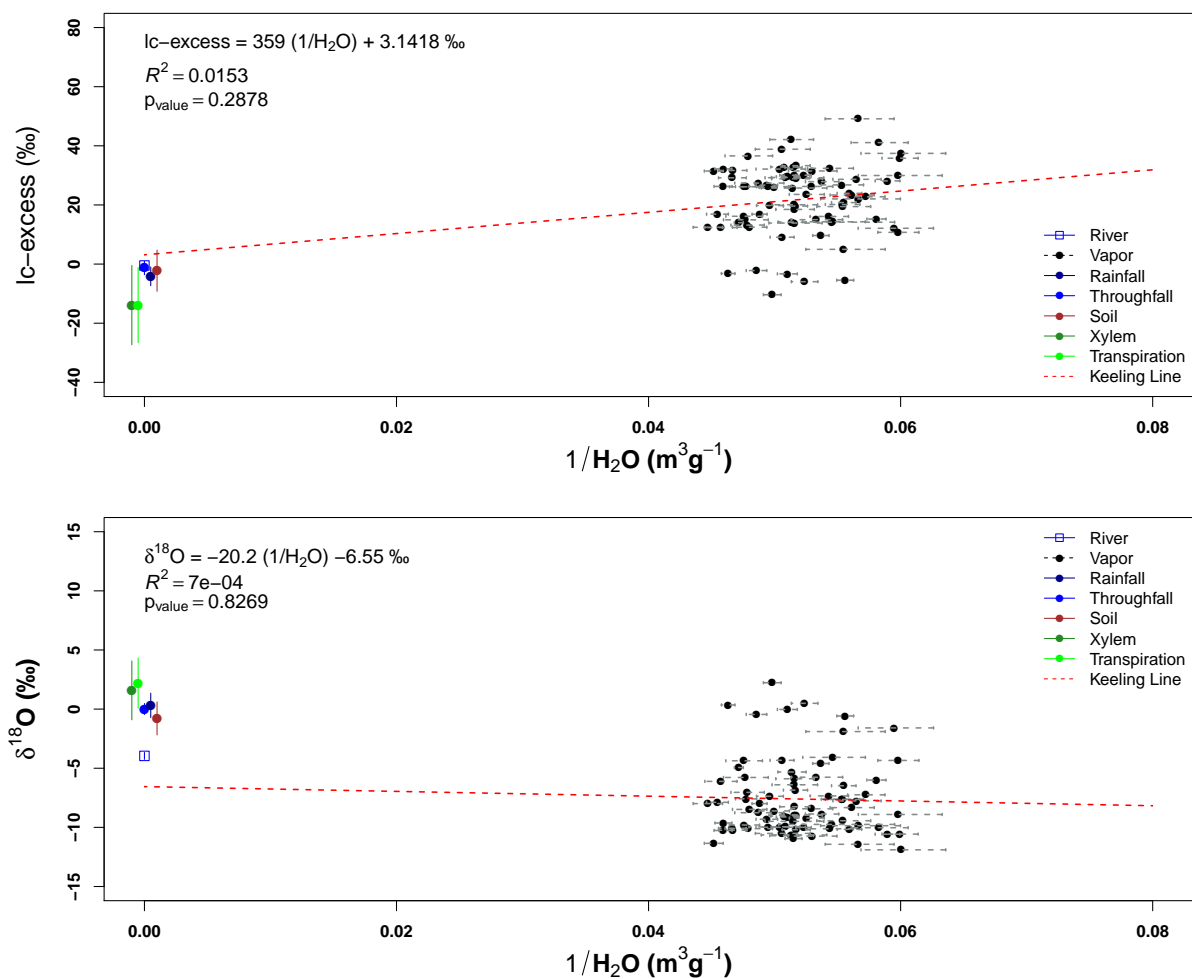
Figure I1. Line-conditioned excess (lc-excess) and oxygen-18 ($\delta^2 O$) mixing relationships ("Keeling plots") for the monitoring period. Air samples collected at 43 m and 22 m height. The standard deviation of each air sample shows the variation of the absolute humidity of the air (ρ_v) for each sampling.

Appendix J: Pairwise comparison

Table J1. Pairwise comparisons to determine differences in lc-excess values among the different sample types. Different colors describe the significance level of the comparison at p=0.05 (green), p=0.01 (blue), p=0.001 (red), and no differences (black).

	P	TF	A-22	A-30	A-43	Stream	X-l	X-b	X-t	X-p	SW-5	SW-10	T-l	T-b	T-p
TF	0.000	-	-	-	-	-	-	-	-	-	-	-	-	-	-
A-22	0.000	0.000	-	-	-	-	-	-	-	-	-	-	-	-	-
A-30	0.000	0.000	0.130	-	-	-	-	-	-	-	-	-	-	-	-
A-43	0.000	0.000	0.491	1.000	-	-	-	-	-	-	-	-	-	-	-
Stream	0.118	1.000	0.098	0.001	0.084	-	-	-	-	-	-	-	-	-	-
X-l	0.040	0.000	0.000	0.000	0.000	0.011	-	-	-	-	-	-	-	-	-
X-b	0.000	0.000	0.000	0.000	0.000	0.024	1.000	-	-	-	-	-	-	-	-
X-t	0.000	0.000	0.000	0.000	0.000	0.002	1.000	1.000	-	-	-	-	-	-	-
X-p	1.000	0.001	0.000	0.000	0.000	0.024	1.000	0.010	0.031	-	-	-	-	-	-
SW-5	0.003	1.000	0.000	0.000	0.000	1.000	0.000	0.000	0.000	0.006	-	-	-	-	-
SW-10	0.002	1.000	0.000	0.000	0.000	1.000	0.001	0.000	0.000	0.008	1.000	-	-	-	-
T-l	0.001	0.000	0.000	0.000	0.000	0.287	0.873	1.000	1.000	0.046	0.000	0.008	-	-	-
T-b	0.027	0.000	0.000	0.000	0.000	0.014	1.000	1.000	1.000	1.000	0.000	0.001	1.000	-	-
T-p	0.346	0.000	0.000	0.000	0.000	0.005	1.000	0.120	0.285	1.000	0.000	0.000	0.196	1.000	-
T-t	0.000	0.000	0.000	0.000	0.000	0.006	1.000	1.000	1.000	0.333	0.000	0.000	1.000	1.000	1.000

P is precipitation. TF is throughfall. A- corresponds to air samples collected at 22 m, 30 m and 43 m. X- and T- correspond to xylem and transpired water, respectively; both sample types collected in lianas (l), bushes (b), palms (p), and trees (t). SW- corresponds to the soil water samples collected at 5 cm and 10 cm depth.